Electronic Supplementary Material (ESI) for Journal of Materials Chemistry C.

Bay-Dissymmetrical Hetero- and Aza-Benzannulated PeryleneDiimides as New n-type Semiconductors

Antoine Goujon,* Lou Rocard, Hayley Melville, Thomas Cauchy, Clément Cabanetos, Sylvie Dabos-Seignon and Piétrick Hudhomme*

Univ Angers, CNRS, MOLTECH-Anjou, SFR MATRIX, F- 49000 Angers, France

antoine.goujon@univ-angers.fr

pietrick.hudhomme@univ-angers.fr

Table of Contents

1. Materials and Methods

Materials and General Methods. Thin Layer Chromatography (TLC) was conducted on pre-coated aluminum sheets with 0.20 mm MerckAlugram SIL G/UV254 with fluorescent indicator UV254. Column chromatography was carried out using Sigma-Aldrich silica gel 60 (particle size 63-200 μm). UV-Vis absorption spectra were recorded on a Shimadzu UV-1800 UV-Vis spectrophotometer using quartz cell (pathlength of 1 cm). Fluorescence was measured on a Shimadzu RF-6000 Spectrophotometer using quartz cell (pathlength of 1 cm). Quantum Yields were measured on a Jasco FP-8500 Spectrophotometer equipped with an ILF-835 integration sphere. Cyclic voltammetry experiments were carried out at room temperature with a Bio-Logic SAS SP-150 potentiostat. ^{1}H and ^{13}C Nuclear Magnetic Resonance (NMR) spectra were obtained on a 500 MHz Advance III HD spectrometer (300 MHz for ^{1}H and 125 MHz for ^{13}C). Chemical shifts were reported in ppm according to tetramethylsilane using the solvent residual signal as an internal reference ($CDCl_3$: δ H= 7.26 ppm). Coupling constants (*J*) were given in Hz. Resonance multiplicity was described as s (singlet), d (doublet), t (triplet), m (multiplet) and br (broad signal). ^{13}C spectra were acquired with a complete decoupling for the proton. High resolution mass spectrometry (HRMS) was performed with a JEOL JMS S3000, MALDI ionisation and SPIRAL TOF detector. Photocyclizations were carried out by introducing the reaction flasks in a photoreactor consisting of 3 x 18 W white LEDs. Atomic Force Microscopy measurements were performed on a Nano-Observer microscope (CSInstruments) under ambient conditions (room temperature, pressure and air). The obtained images were processed with the open access sotfware Gwyddion. Gaussian (09 revision D.01) was used to perform the DFT calculations. Chemicals were purchased from Sigma Aldrich, Acros Organics, Fisher Scientific, Alfa Aesar, Fluorochem, and were used as received. Solvents were purchased from Sigma Aldrich, Fluorochem, or Fischer Scientific, deuterated solvents from Sigma Aldrich. Photocyclizations were performed using a lamp equipped of 3 x 7W white LEDs.

Abbreviations. AFM : Atomic Force Microscopy, AzaBPDI : AzaBenzannulated Perylenediimide; DMF : N,N-Dimethylformamide; DDQ : 2,3-dichloro-5,6-dicyanobenzoquinone; DFT : density functional theory; HOMO : highest occupied molecular orbital; HRMS : high resolution mass spectrometry; LUMO : lowest unoccupied molecular orbital; NMR : Nuclear Magnetic Resonance; PDI : perylenediimide; RMS : Root Mean square roughness; rt : room temperature; TFA : Trifluoroacetic Acid; THF : tetrahydrofuran.

2. Synthesis

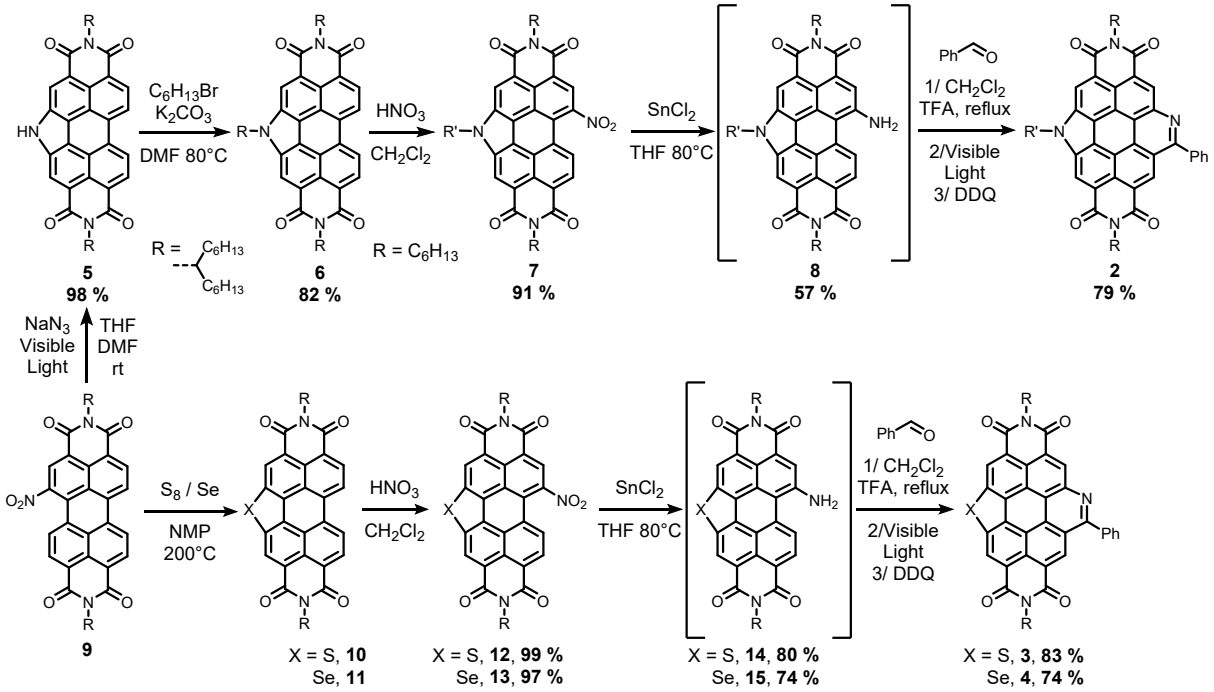

Scheme S1. Synthesis of AzaBPDIs **2**, **3** and **4**.

Compound 1. This dye was prepared according to previously reported procedure.[1]

Compound 5. NitroPDI **9**[1] (500 mg, 0.65 mmol) was dissolved in THF/DMF 1:1 (20 mL). NaN_3 (50 mg, 0.78 mmol) was added and the mixture was stirred at rt while being exposed to 3 x 18W white LEDs. Full conversion into the annulated compound was observed by TLC after 30 min. Water (50 mL) was added and the mixture was extracted with CH_2Cl_2 (3 x 30 mL). The organic phases were combined, dried ($MgSO_4$) and concentrated under reduced pressure, affording compound **5** as a red solid (488 mg, 98%). Spectroscopic characterizations were in accordance with the literature.[2]

Compound 6. N-annulated PDI **5** (328 mg, 0.43 mmol) and K_2CO_3 (138 mg, 1.28 mmol) were suspended in anhydrous DMF (10 mL) under argon. 1-Bromohexane (127 µL, 0.86 mmol) was added and the reaction mixture was stirred overnight at 80 °C. Water (20 mL) was added and the mixture was extracted with CH_2Cl_2 (3 x 20 mL). The organic phases were combined, washed with brine, dried ($MgSO_4$) and concentrated under reduced pressure. The residue was purified through silica gel column chromatography (eluent: CH_2Cl_2/Petroleum Ether 1:1) affording compound **6** as a red oily solid (300 mg, 82%). NMR spectra display a mixture of conformers. ^{1}H NMR (500 MHz, $CDCl_3$, ppm): δ 8.81 (br *s*, 2H), 8.74-8.63 (m, 4H), 5.40-5.25 (m, 4H), 4.77-4.63 (m, 4H), 2.40-2.30 (m, 4H), 2.14-2.06 (m, 2H), 2.02-1.92 (m, 4H),

1.50-1.29 (m, 20H), 1.29-1.17 (m, 17H), 0.87-0.74 (m, 12H). ^{13}C NMR (125 MHz, $CDCl_3$, ppm): δ 166.4, 165.3, 165.1, 164.1, 134.6, 132.4, 128.1, 127.4, 124.5, 123.6, 122.8, 122.3, 122.1, 121.6, 119.2, 119.0, 118.3, 54.9, 46.9, 32.7, 31.9, 31.6, 31.4, 29.4, 26.9, 22.7, 22.5, 14.1, 14.0. HRMS calcd. for $C_{56}H_{73}N_3O_4$ ($[M]^-$): 851.5606 found: 851.5610 (0.40 ppm error).

Compound 7. To a solution of PDI(Nhex) **6** (620 mg, 0.73 mmol) in CH_2Cl_2 (50 mL), fuming nitric acid (0.31 mL, 7.4 mmol) was added. The reaction mixture was stirred at rt and monitored by TLC until the mononitration was achieved (around 15 min). The mixture was poured into H_2O (100 mL) and the aqueous phase was extracted with CH_2Cl_2 (2 x 50 mL). The combined organic phases were dried ($MgSO_4$) and concentrated under reduced pressure. The residue was purified on silica gel column chromatography (eluent: CH_2Cl_2 / Petroleum ether 1:1) to afford **7** as a red solid (595 mg, 91%). NMR spectra display a mixture of conformers. ^{1}H NMR (500 MHz, $CDCl_3$, ppm): δ 9.18 and 9.14 (two *s*, 1H), 9.09 and 9.05 (*two s*, 1H), 8.93 and 8.88 (*two s*, 1H), 8.84-8.81 (*m*, 2H), 5.31 (*br*, 2H), 4.95 (*br*, 2H), 2.36-2.28 (*m*, 4H), 2.27-2.21 (*m*, 2H), 1.97-1.87 (*m*, 4H), 1.49-1.21 (*m*, 38H), 0.87 (*t*, 3H), 0.83-0.80 (*m*, 12H). ^{13}C NMR (125 MHz, $CDCl_3$, ppm): δ 166.3, 166.0, 165.2, 164.8, 163.9, 163.7, 162.7, 147.2, 135.6, 135.0, 128.7, 127.9, 127.7, 125.7, 124.9, 124.1, 123.2, 123.0, 122.9, 122.5, 122.5, 122.2, 121.7, 121.2, 120.5, 119.6, 119.3, 118.9, 55.5, 55.3, 47.4, 32.7, 32.5, 31.9, 31.8, 31.5, 29.4, 29.4, 27.1, 27.1, 27.0, 22.7, 22.6, 14.2, 14.1. HRMS calcd. for $C_{56}H_{72}N_4O_6$ ($[M]^-$): 896.5457 found: 896.5455 (0.25 ppm error).

Compound 2. To a solution of nitroPDI(Nhex) **7** (232 mg, 0.26 mmol) in anhydrous THF (20 mL) under argon, $SnCl_2.2H_2O$ (584 mg, 2.60 mmol) was added along with 2 drops of concentrated 12N HCl. The reaction mixture was stirred at 80 °C for 6 h and was poured into an aqueous solution of 2N NaOH (20 mL). The aqueous phase was extracted with CH_2Cl_2 (3 x 50 mL). The combined organic phases were dried ($MgSO_4$) and concentrated under reduced pressure. The residue was purified on silica gel column chromatography (eluent: CH_2Cl_2 then CH_2Cl_2/MeOH 97:3) to afford amine derivative **8** as a purple solid (128 mg, 57%). To a solution of aminoPDI(Nhex) **8** (50 mg, 0.06 mmol) in CH_2Cl_2 (3 mL), benzaldehyde (19 mg, 0.18 mmol) and TFA (three drops) were added. The reaction mixture was stirred at reflux for 2 h and was diluted with CH_2Cl_2 (60 mL). The mixture was stirred at rt overnight while exposed to visible light (white LED, 7 W), then DDQ (12 mg, 0.06 mmol) was added. After stirring 2 min, the solvent was evaporated and the crude was purified on silica gel column chromatography (eluent: CH_2Cl_2) and precipitated into CH_2Cl_2/MeOH to afford **2** as a red solid (45 mg, 79%). NMR spectra display a mixture of conformers. ^{1}H NMR (500 MHz, $CDCl_3$, ppm): δ 9.82 and 9.78

(*two s*, 1H), 9.77 and 9.72 (*two s*, 1H), 9.42 and 9.37 (*two s*, 1H), 9.34 and 9.29 (*two s*, 1H), 8.30 (*d*, *J* = 7.8 Hz, 2H), 7.80 (*t*, *J* = 7.8 Hz, 2H), 7.73 (*t*, *J* = 7.8 Hz, 1H), 5.47-5.39 (*m*, 2H), 5.06 (*br*, 2H), 2.43-2.35 (*m*, 6H), 2.03-1.97 (*m*, 4H), 1.67-1.60 (*m*, 2H), 1.47-1.19 (*m*, 36H), 0.90 (*t*, 3H), 0.82-0.77 (*m*, 12H). ^{13}C NMR (125 MHz, $CDCl_3$, ppm): δ 167.0, 166.8, 165.9, 165.9, 165.7, 164.8, 164.6, 162.4, 144.7, 140.2, 139.7, 138.6, 131.3, 130.3, 130.0, 129.4, 129.2, 128.7, 128.4, 126.5, 125.6, 124.4, 124.3, 124.0, 123.7, 123.6, 123.5, 122.9, 122.6, 122.1, 122.0, 121.8, 120.7, 120.3, 119.5, 118.2, 117.4, 116.6, 115.9, 55.5, 55.4, 47.6, 32.9, 32.8, 31.9, 31.7, 31.6, 29.4, 27.2, 27.2, 27.2, 22.7, 22.7, 14.2, 14.2, 14.1. HRMS calcd. for $C_{63}H_{77}N_4O_4$ ($[M+H]^+$): 953.5939 found: 953.5936 (0.26 ppm error).

Compound 12. To a solution of compound **10**[3] (200 mg, 0.26 mmol) in CH_2Cl_2 (15 mL), fuming nitric acid (110 µL, 2.6 mmol) was added. The reaction mixture was stirred at rt and monitored by TLC until the mononitration was achieved (around 15 min). The mixture was poured into H_2O (200 mL), and the aqueous phase was extracted with CH_2Cl_2 (2 x 100 mL). The combined organic phases were dried ($MgSO_4$) and concentrated under reduced pressure. The residue was taken back into minimum of CH_2Cl_2 and methanol was added. The precipitate was filtered and compound **12** was obtained as a red solid (210 mg, 99%). ^{1}H NMR (500 MHz, $CDCl_3$, ppm): δ 9.47-9.24 (m, 2H), 8.82 (br m, 2H), 8.61-8.47 (m, 1H), 5.31-5.23 (br m, 2H), 2.37-2.24 (m, 4H), 1.97-1.88 (m, 4H), 1.42-1.27 (m, 16H), 1.27-1.15 (m, 16H), 0.86-0.76 (m, 12H). ^{13}C NMR (125 MHz, $CDCl_3$, ppm): δ 164.9, 164.5, 164.2, 163.6, 163.3, 163.1, 162.1, 146.9, 139.1, 138.9, 131.1, 130.5, 130.3, 129.6, 128.9, 128.4, 127.9, 127.2, 126.9, 126.8, 126.1, 124.5, 124.3, 124.3, 124.1, 124.0, 123.8, 123.7, 123.5, 123.4, 123.3, 123.2, 123.0, 122.3, 55.6, 55.4, 32.5, 32.4, 31.9, 29.3, 29.3, 27.1, 27.1, 22.7, 14.1. HRMS calcd. for $C_{50}H_{59}N_3O_6S$ ($[M]^-$): 829.4130 found: 829.4131 (0.06 ppm error).

Compound 3. To a solution of compound **12** (50 mg, 0.06 mmol) in anhydrous THF (5 mL) under argon, $SnCl_2.2H_2O$ (114 mg, 0.6 mmol) was added along with 2 drops of concentrated 12N HCl. The reaction mixture was stirred at 80 °C for 6 h and was poured into an aqueous solution of 2N NaOH (20 mL). The aqueous phase was extracted with CH_2Cl_2 (3 x 20 mL). The combined organic phases were dried ($MgSO_4$) and concentrated under reduced pressure. The residue was purified on silica gel column chromatography (eluent: CH_2Cl_2 then CH_2Cl_2/MeOH 97:3) to afford the amino derivative **14** as a purple solid (38 mg, 80%). Because of its instability, compound **14** was engaged immediately in the next step. To a solution of compound **14** (38 mg, 0.05 mmol) in CH_2Cl_2 (5 mL), benzaldehyde (15.2 µL, 0.15 mmol) and TFA (three drops) were added. The reaction mixture was stirred at reflux for 2 h and was diluted

with CH_2Cl_2 (15 mL). The mixture was stirred at rt overnight while exposed to visible light (white LED, 7 W), and DDQ (11 mg, 0.05 mmol) was added. After stirring 2 min, the solvent was evaporated and the crude was purified on silica gel column chromatography (eluent CH_2Cl_2) and precipitated into CH_2Cl_2/MeOH to afford compound **3** as a red solid (36 mg, 83%). ^{1}H NMR (500 MHz, $CDCl_3$, ppm): δ 9.85-9.54 (m, 4H), 8.18 (*d*, *J* = 6.7 Hz, 2H), 7.81 (*t*, *J* = 7.8 Hz, 2H), 7.81 (*t*, *J* = 7.4 Hz, 1H), 5.47-5.35 (br m, 2H), 2.49-2.33 (m, 4H), 2.12-1.93 (m, 4H), 1.57-1.32 (m, 16H), 1.32-1.20 (m, 16H), 0.93-0.76 (m, 12H). ^{13}C NMR (125 MHz, $CDCl_3$, ppm): δ 165.5, 165.1, 164.3, 164.0, 162.4, 144.0, 140.5, 140.0, 138.4, 132.0, 131.3, 131.1, 131.0, 130.8, 130.2, 130.1, 130.0, 129.4, 129.3, 127.5, 127.1, 126.3, 126.0, 125.3, 124.5, 124.2, 123.9, 123.6, 123.1, 122.7, 122.6, 122.0, 121.8, 119.0, 118.9, 116.9, 55.7, 55.6, 32.7, 31.9, 29.4, 27.3, 22.7, 14.2. HRMS calcd. for $C_{57}H_{64}N_3O_4S$ ($[M+H]^+$): 886.4612 found: 886.4614 (0.07 ppm error).

Compound 13. To a solution of compound **11**[4] (126 mg, 0.15 mmol) in CH_2Cl_2 (10 mL), fuming nitric acid (61 µL, 1.5 mmol) was added. The reaction mixture was stirred at rt and monitored by TLC until the mononitration was achieved (around 15 min). The mixture was poured into H_2O (200 mL), and the aqueous phase was extracted with CH_2Cl_2 (2 x 100 mL). The combined organic phases were dried ($MgSO_4$) and concentrated under reduced pressure. The residue was taken back into minimum of CH_2Cl_2 and methanol was added. The precipitate was filtered affording compound **13** as a red solid (128 mg, 97%). ^{1}H NMR (500 MHz, $CDCl_3$, ppm): δ 9.50-9.28 (m, 2H), 8.82 (br m, 2H), 8.60-8.46 (m, 1H), 5.32-5.20 (br m, 2H), 2.36-2.23 (m, 4H), 1.96-1.85 (m, 4H), 1.42-1.27 (m, 16H), 1.27-1.18 (m, 16H), 0.84-0.79 (m, 12H). ^{13}C NMR (125 MHz, $CDCl_3$, ppm): δ 164.8, 164.5, 164.3, 163.6, 163.1, 162.1, 146.8, 141.9, 141.7, 134.1, 133.3, 132.0, 131.3, 130.4, 130.3, 129.6, 128.6, 127.0, 126.6, 126.4, 125.3, 124.7, 124.5, 124.0, 123.8, 123.6, 123.4, 123.3, 122.7, 122.2, 121.5, 55.6, 55.3, 32.5, 32.4, 31.9, 29.3, 27.1, 22.7, 14.1. HRMS calcd. for $C_{50}H_{59}N_3O_6Se$ ($[M]^-$): 877.3575 found: 877.3566 (0.99 ppm error).

Compound 4. To a solution of compound **13** (50 mg, 0.06 mmol) in anhydrous THF (5 mL) under argon, $SnCl_2.2H_2O$ (114 mg, 0.6 mmol) was added along with 2 drops of concentrated 12N HCl. The reaction mixture was stirred at 80 °C for 6 h and was poured into an aqueous solution of 2N NaOH (20 mL). The aqueous phase was extracted with CH_2Cl_2 (3 x 20 mL). The combined organic phases were dried ($MgSO_4$) and concentrated under reduced pressure. The residue was purified on silica gel column chromatography (eluent: CH_2Cl_2 then CH_2Cl_2/MeOH 97:3) to afford the amino derivative **15** as a purple solid (35 mg, 74%). Because of its instability, compound **15** was engaged immediately in the next step. To a solution of

compound **15** (35 mg, 0.04 mmol) in CH_2Cl_2 (5 mL), benzaldehyde (13.5 µL, 1.2 mmol) and TFA (three drops) were added. The reaction mixture was stirred at reflux for 2 h and was diluted with CH_2Cl_2 (15 mL). The mixture was stirred at rt overnight while exposed to visible light (white LED, 7 W), then DDQ (10 mg, 0.04 mmol) was added. After stirring 2 min, the solvent was evaporated and the crude was purified on silica gel column chromatography (eluent: CH_2Cl_2) and precipitated into CH_2Cl_2/MeOH to afford compound **4** as a red solid (32 mg, 88%). ^{1}H NMR (500 MHz, $CDCl_3$, ppm): δ 9.83-9.51 (m, 4H), 8.15 (*d*, *J* = 6.2 Hz, 2H), 7.81 (*t*, *J* = 7.8 Hz, 2H), 7.75 (*t*, *J* = 7.6 Hz, 1H), 5.46-5.33 (br m, 2H), 2.48-2.31 (m, 4H), 2.09-1.96 (m, 4H), 1.52-1.33 (m, 16H), 1.33-1.21 (m, 16H), 0.86-0.79 (m, 12H). ^{13}C NMR (125 MHz, $CDCl_3$, ppm): δ 165.1, 164.8, 163.9, 163.6, 161.9, 143.5, 141.5, 140.9, 138.1, 133.3, 132.5, 132.0, 131.3, 130.9, 130.6, 129.9, 129.1, 128.3, 127.4, 124.9, 124.1, 123.5, 122.8, 122.6, 122.1, 121.8, 121.6, 120.8, 120.0, 119.9, 116.8, 55.4, 55.3, 32.5, 31.7, 29.2, 27.0, 22.5, 13.9. HRMS calcd. for $C_{57}H_{64}N_3O_4Se$ ($[M+H]^+$): 934.4057 found: 934.4072 (1.70 ppm error).

3. Thermogravimetric Analysis

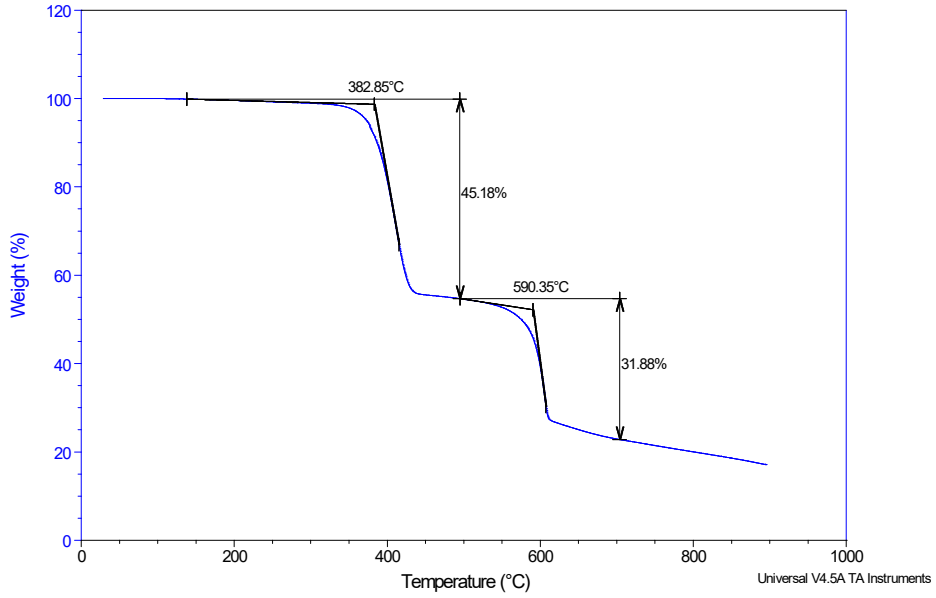

Figure S1. Thermogravimetric analysis of compound **1**.

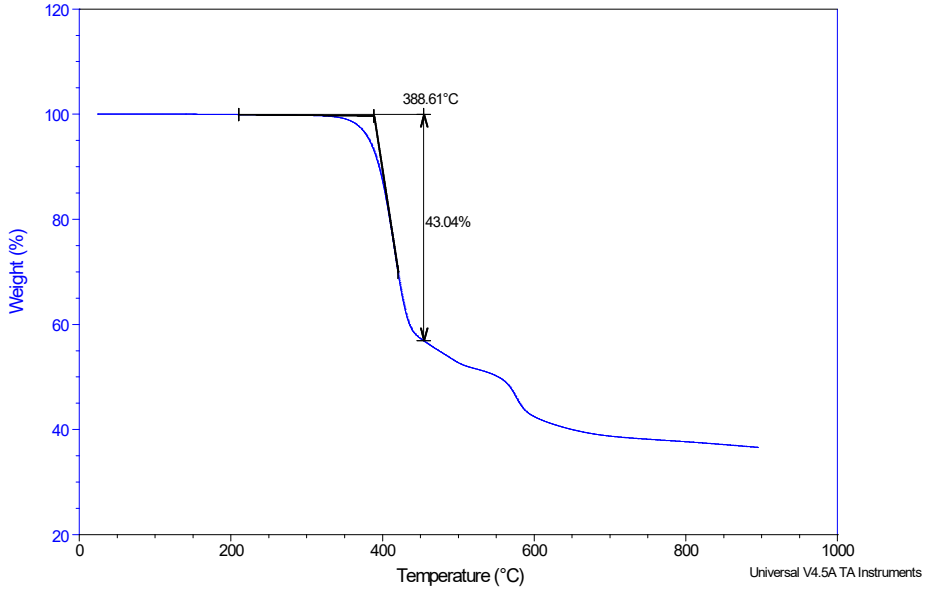

Figure S2. Thermogravimetric analysis of compound **2.**

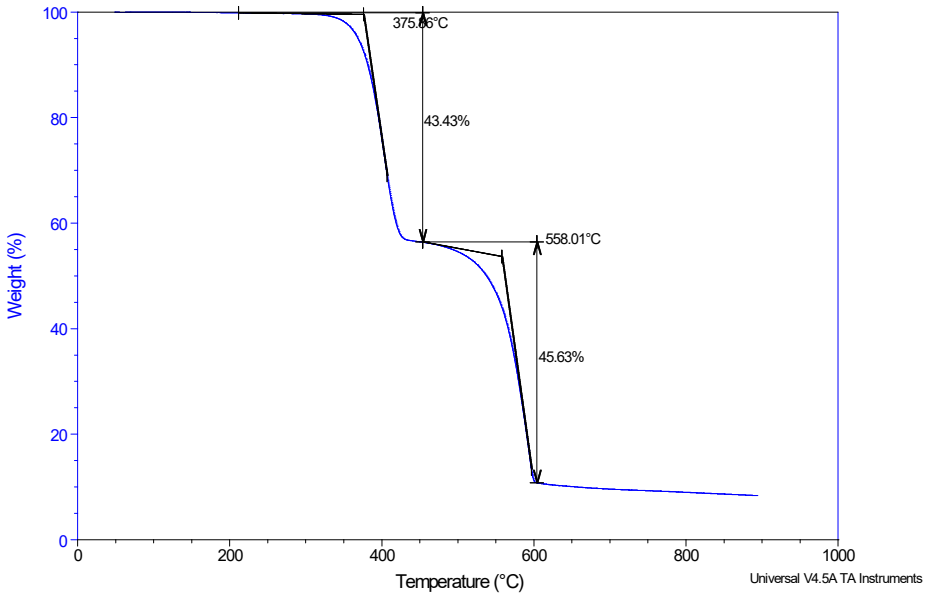

Figure S3. Thermogravimetric analysis of compound **3.**

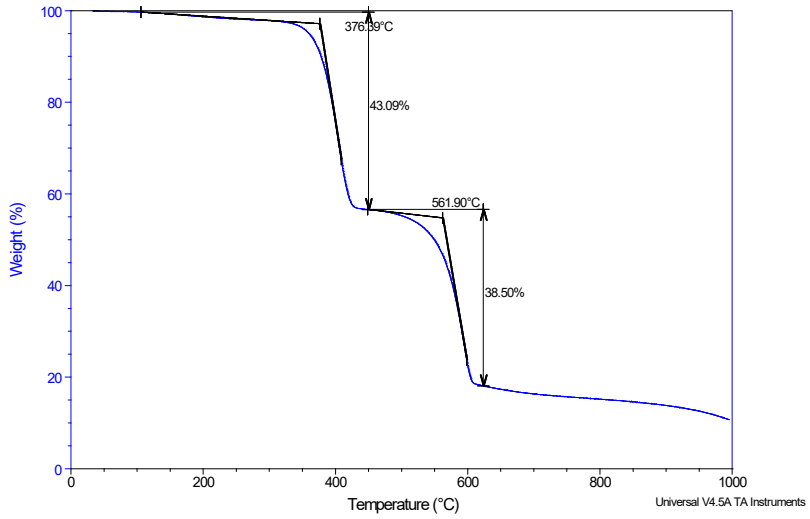

Figure S4. Thermogravimetric analysis of compound **4.**

4. Electrochemistry

Cyclic voltammetry was carried out on a Bio-Logic SAS SP-150 potentiostat with a three electrodes configuration, using a silver wire as Ag/AgCl reference electrode, a Pt wire as counter electrode, and a Pt electrode as working electrode. Samples (C = 5.10^{-4} M) were dissolved in a 0.1 M Bu_4NPF_6 solution in CH_2Cl_2 as supporting electrolyte and ferrocene was used as internal reference. The scan rate is 100 $mV.s^{-1}$. The solutions were degassed by bubbling argon for 30 s before measurements.

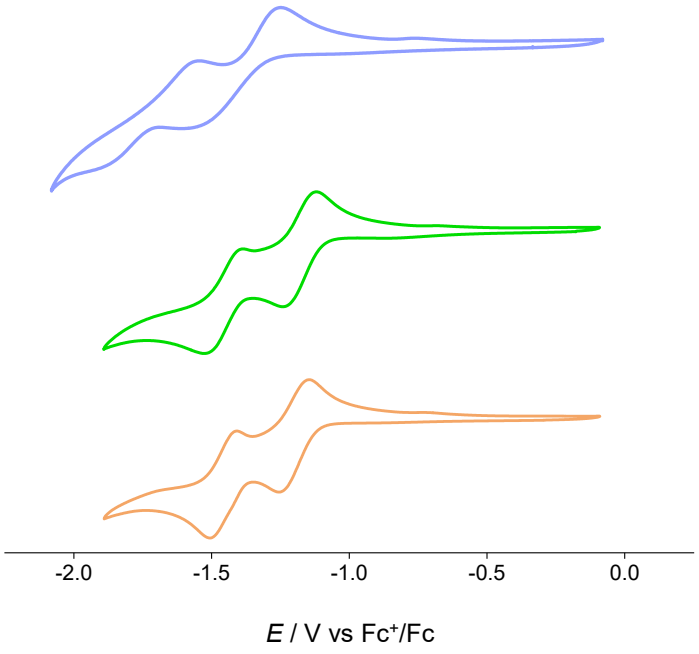

Figure S5. Cyclic voltammogram of compound **2**, **3**, and **4** (in that order from top to bottom). V *vs* Fc^+/Fc.

5. Summary of Optical and Electronic Properties

	1	2	3	4
$\lambda_{ab}(S_0\text{-}S_1)$ / nm[a]	474	505	481	489
$\varepsilon/10^3$ $M^{-1}cm^{-1}$[b]	67.2	36.6	24.7	25.5
λ_{em} / nm	486	514	491	499
Φ_f[c]	0.83	0.50	0.09	0.01
$E^{red1}_{1/2}$/V[d]	-1.13	-1.40	-1.17	-1.21
LUMO exp[e] / eV	-3.67	-3.40	-3.63	-3.59
LUMO calc / eV	-3.63	-3.41	-3.62	-3.60
HOMO exp[f] / eV	-6.25	-5.80	-6.14	-6.06
HOMO calc / eV	-6.47	-6.31	-6.57	-6.52

Table S1. Optical and electronic properties of dyes **1**, **2**, **3** and **4**. Absorption and emission spectra, reduction potentials data recorded in CH_2Cl_2 at rt. [a]Maximum wavelength of the lowest energy absorption band. [b]Extinction coefficient of the lowest energy absorption band. [c]Fluorescence Quantum Yields measured with an integration sphere. [d]Recorded using 0.1 M *n*-Bu_4PF_6. [e]Calculated from the formula $E^{LUMO} = -[E^{red1}_{1/2} + 4.8]$ eV. [f]Calculated from the formula $E^{HOMO} = [E^{LUMO} - E^{OptGap}]$ eV.

Figure S6. Energy diagram of experimental (solid lines) and computed (dotted lines) energy levels of HOMO and LUMO orbitals of compounds **1** (yellow), **2** (blue), **3** (green), and **4** (orange).

6. UV-Visible Spectroscopy on Thin Films

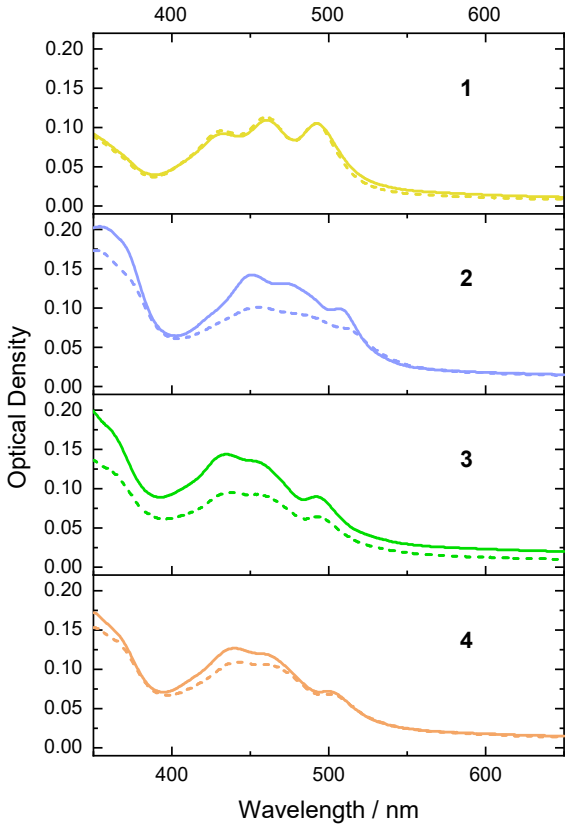

Figure S7. Absorption spectra of AzaBPDIs spin-coated from 10 mg/mL chloroform solutions on glass substrates before (solid line) and after (dashed line) thermal annealing (100 °C, 10 min).

7. Space-Charge-Limited-Current Measurements

Preparation of electron-only devices for SCLC measurements. The device architecture was as follow: glass/ITO/ZnO/active layer/Al. ZnO was used as the electron transporting layer. Two sets of devices were prepared for each compound: one was measured as prepared; the second one was thermally annealed at 100 °C for 20 min before Al deposition. The I-V curves were recorded from 0 to 10 V in a glove-box. The film thickness was then measured by profilometry. ITO-patterned glass substrates were purchased from VisionTek Systems Ltd. (25 mm x 24 mm x 1.1 mm, sheet resistance = 10 Ω/sq) and cleaned in an ultrasonic bath for 4 subsequent 15 minute intervals; first in deoinised water and several drops of detergent (Deconex® 12 PA-x solution), deionised water alone, acetone and finally ethanol. The substrates were then dried with hot air and further cleaned with a UV-ozone treatment for 15 minutes (UV Ozone cleaner, Ossila). In details, the ZnO stock solution[5] was stirred overnight at 45 °C. The solution was spin-coated on glass-ITO substrates (80 µL, 2000 rpm). The substrates were annealed at 180 °C for one hour before the active layer (3 $mg.mL^{-1}$ in $CHCl_3$)

was deposited by spin-coating (80 µL, 1500 rpm). Then, the 100 nm aluminium electrode was deposited *via* physical vapour deposition at a vacuum of 1×10^{-6} mbar before introducing the finished devices into a glovebox. The electron mobility μ_e was extracted using the Mott-Gurney law by fitting the linear SCLC regime of the $I=f(V^2)$ plot represented in logarithmic scale.

AzaBPDIs	**1**	**3**	**4**
μ_e in $cm^2\ V^{-1}\ s^{-1}$ (thickness in nm) No annealing	5.12×10^{-3} (126)	1.13×10^{-3} (76)	7.05×10^{-4} (65)
μ_e in $cm^2\ V^{-1}\ s^{-1}$ (thickness in nm) Annealed	4.10×10^{-3} (117)	2.13×10^{-3} (94)	1.04×10^{-3} (74)

Table S2. Electron mobilities for compounds **1**, **3** and **4** measured by SCLC in electrons-only devices with or without thermal annealing at 100 °C. The thickness of each active layer, measured by profilometry, is displayed in parenthesis.

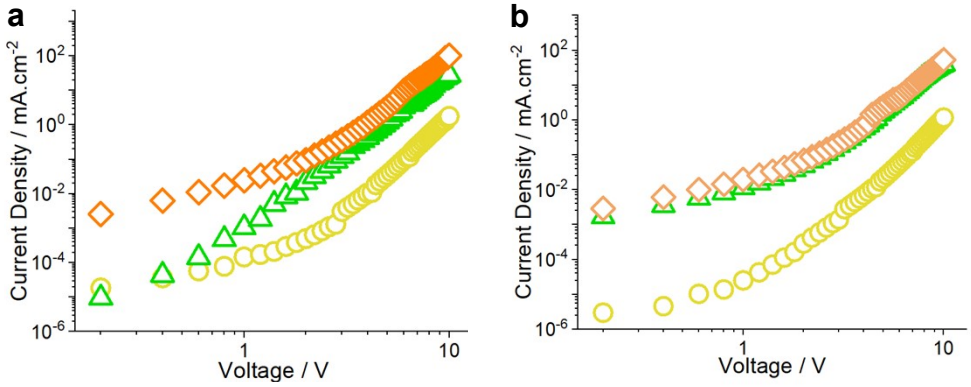

Figure S8. Typical I/V curves recorded for electrons-only devices of compounds **1** (yellow circles), **3** (green triangles) and **4** (orange diamonds) a) before and b) after thermal annealing.

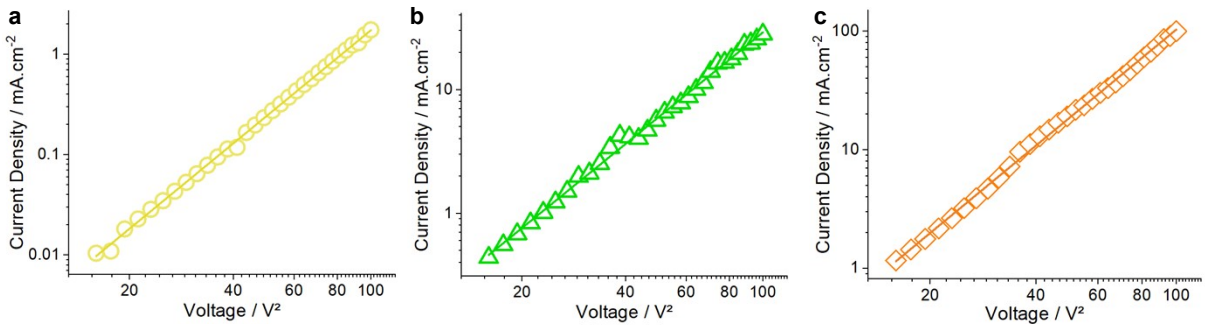

Figure S9. I as a function of V^2 in the SCLC regime represented in logarithmic scale, recorded in electron-only devices with thin films of **1** (a), **3** (b) and **4** (d).

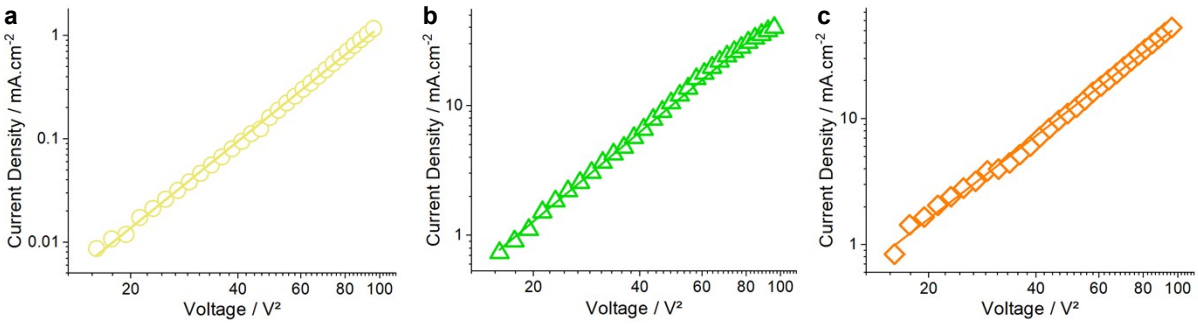

Figure S10. I as a function of V^2 in the SCLC regime represented in logarithmic scale, recorded in thermally annealed electron-only devices with thin films of **1** (a), **3** (b) and **4** (d).

8. Atomic Force Microscopy

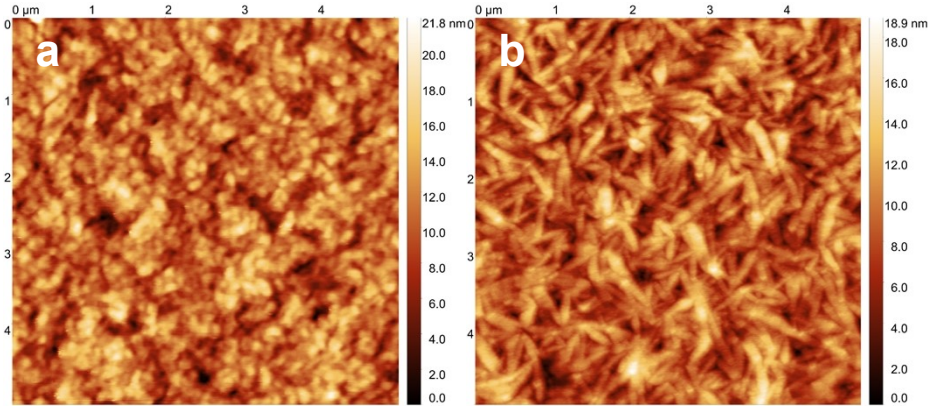

Figure S11. AFM imaging of films of compound **1** in SCLC devices (a) before and (b) after thermal annealing.

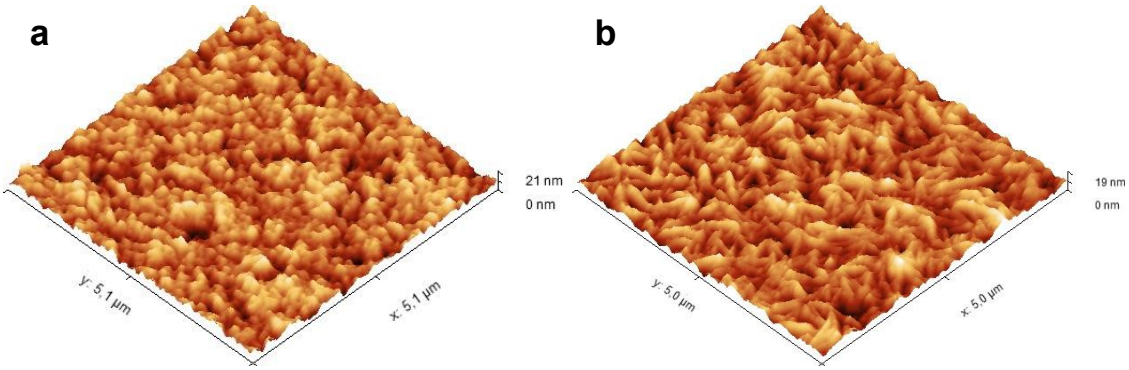

Figure S12. AFM imaging of films of compound **1** in SCLC devices (a) before and (b) after thermal annealing.

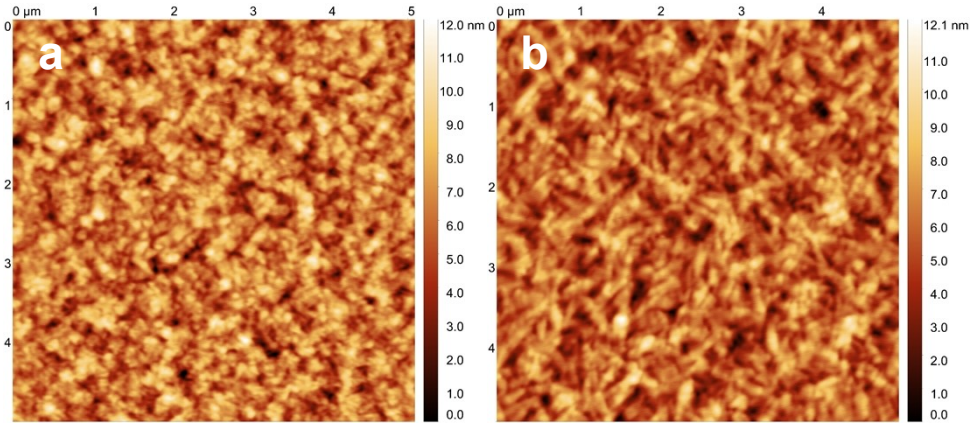

Figure S13. AFM imaging of films of compound **3** in SCLC devices (a) before and (b) after thermal annealing.

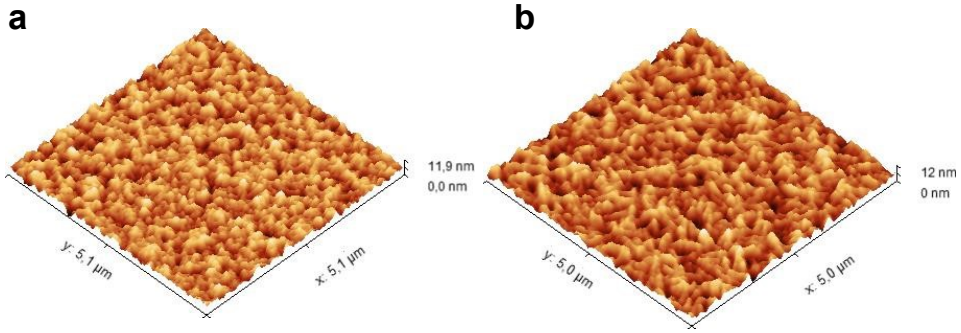

Figure S14. AFM imaging of films of compound **3** in SCLC devices (a) before and (b) after thermal annealing.

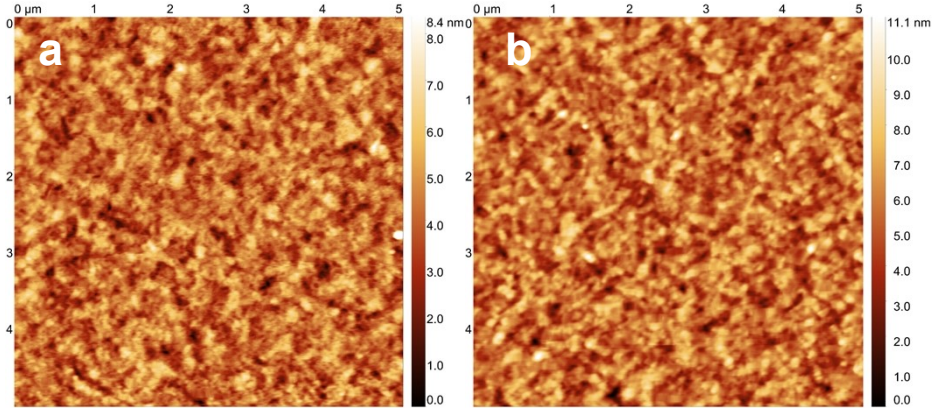

Figure S15. AFM imaging of films of compound **4** in SCLC devices (a) before and (b) after thermal annealing.

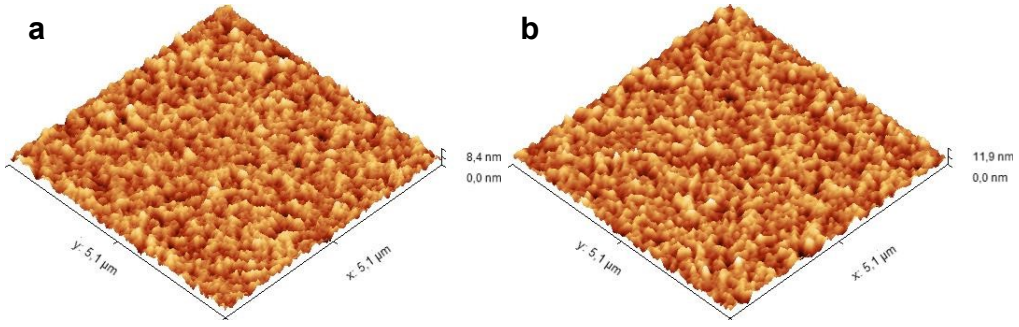

Figure S16. AFM imaging of films of compound **4** in SCLC devices (a) before and (b) after thermal annealing.

Compound	1	3	4
Before Annealing	1.87	1.67	0.91
After Annealing	5.68	1.60	1.30

Table S3. RMS (determine on 20 µm x 20 µm images) in nm of films in SCLC devices before and after thermal annealing measured by AFM.

9. X-Ray Diffraction on Thin Films

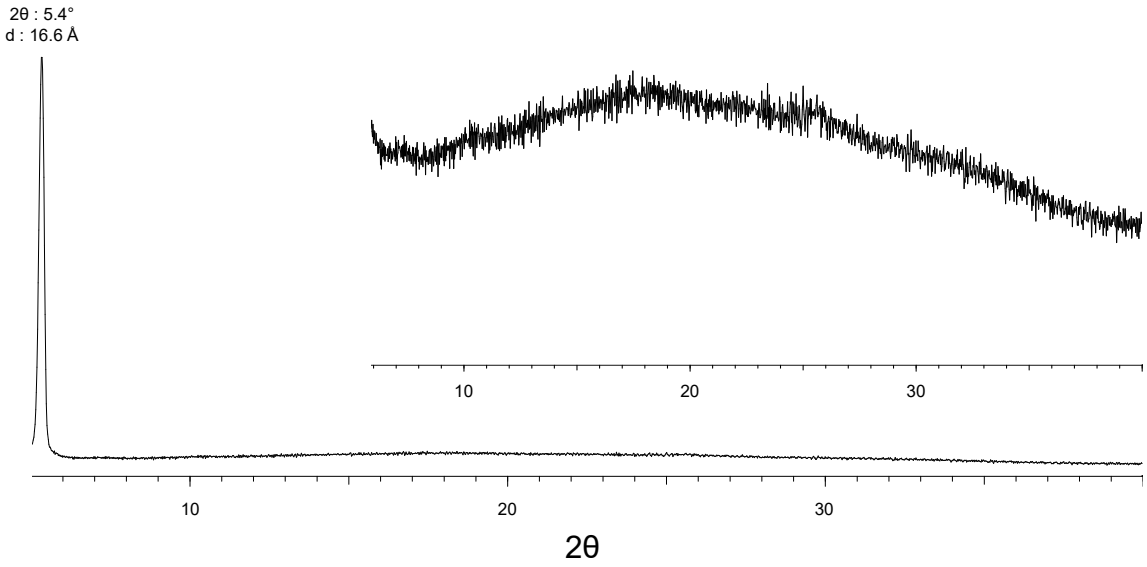

Figure S17. X-ray diffraction of the film from compound **1**.

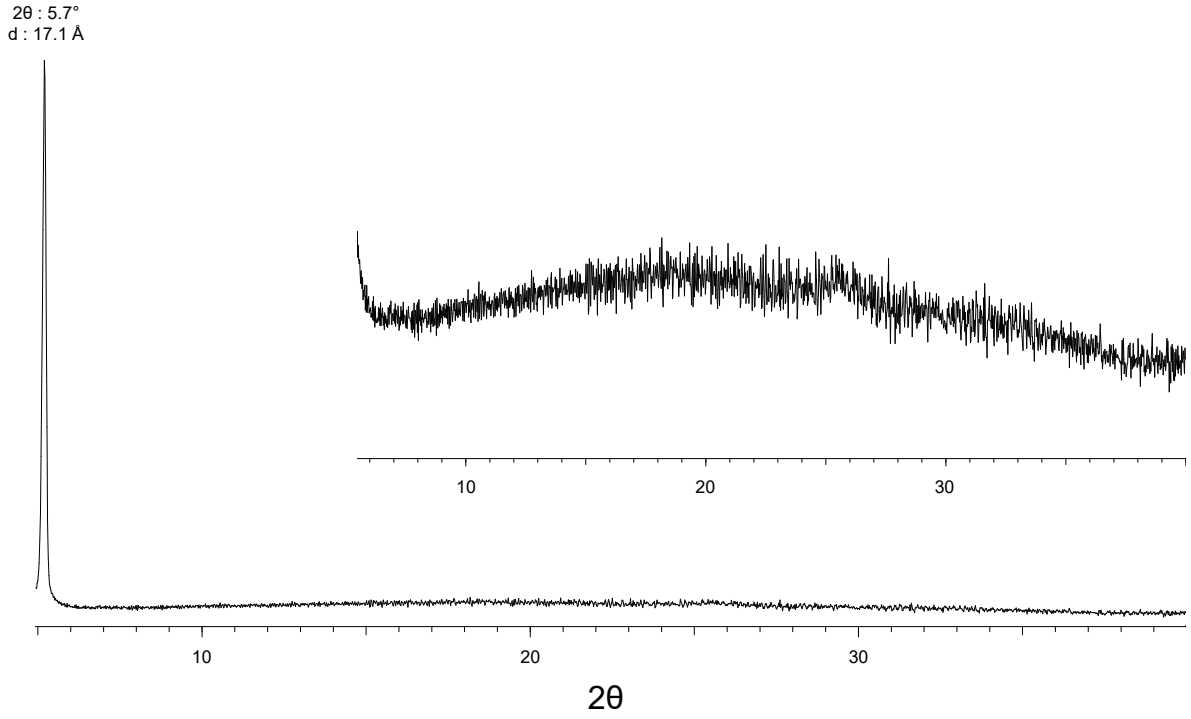

Figure S18. X-ray diffraction of the film from compound **1** after thermal annealing (20 min at 100 °C).

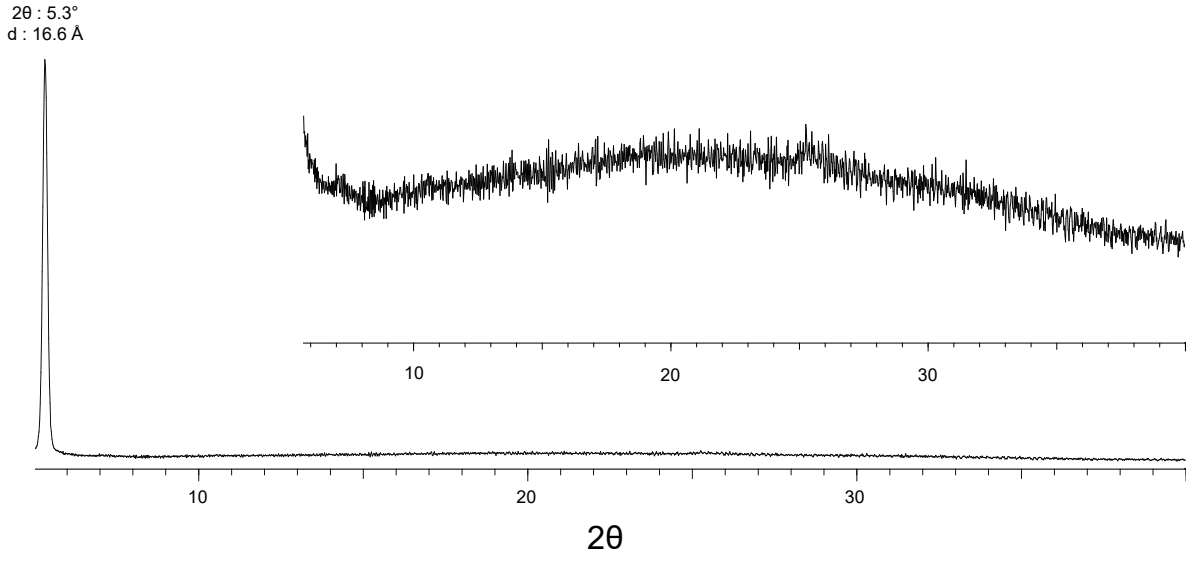

Figure S19. X-ray diffraction of the film from compound **3**.

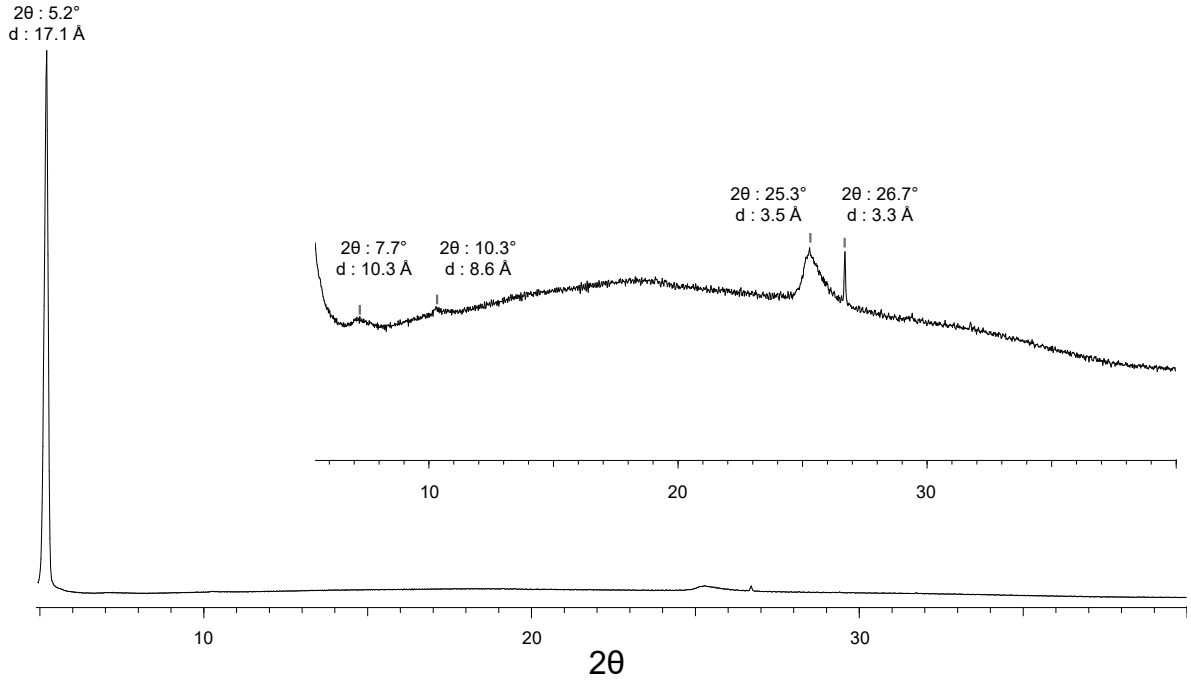

Figure S20. X-ray diffraction of the film from compound **3** after thermal annealing (20 min at 100 °C).

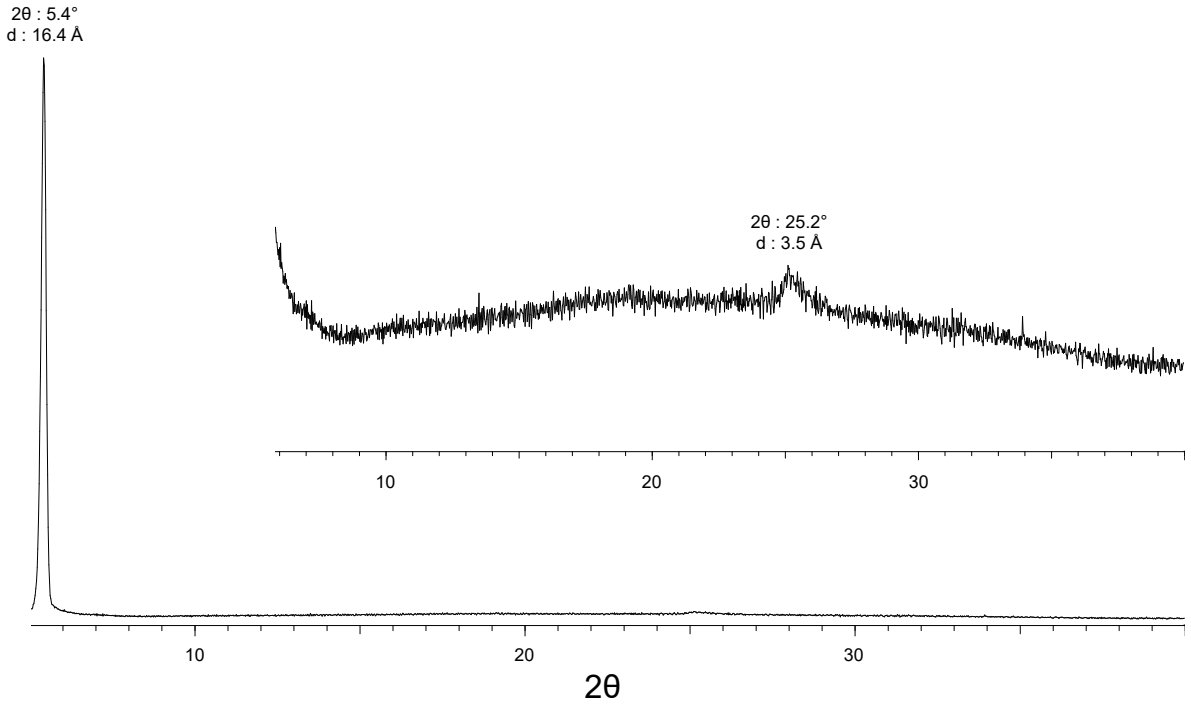

Figure S21. X-ray diffraction of film of compound **4**.

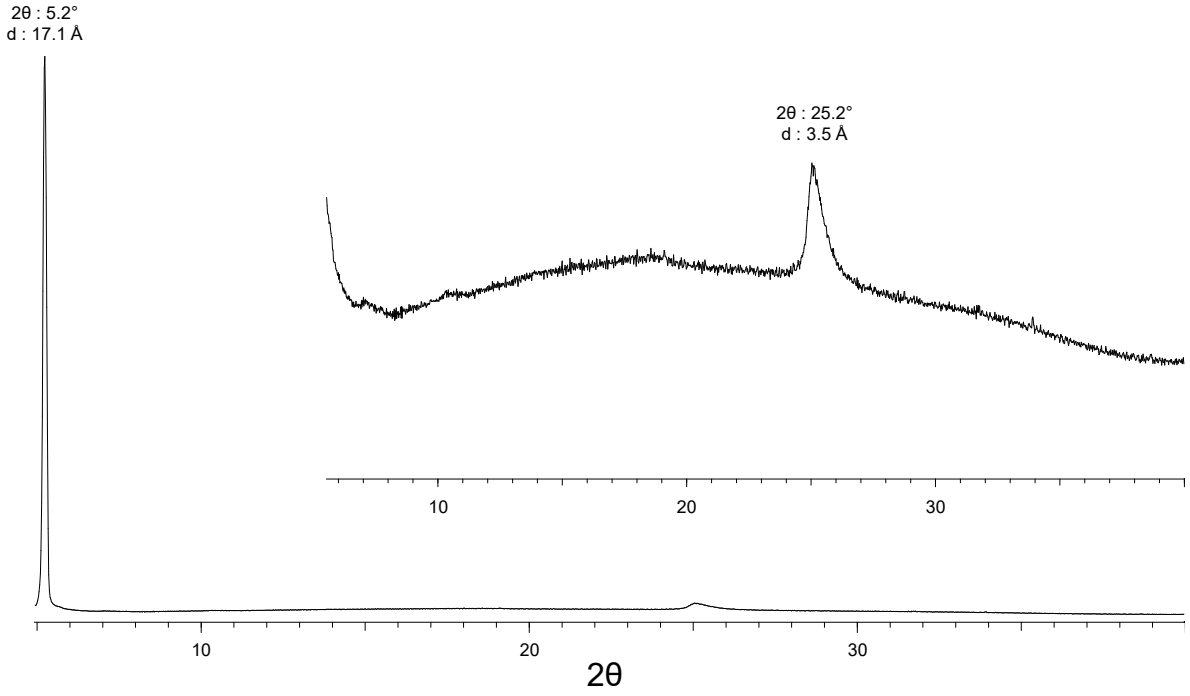

Figure S22. X-ray diffraction of the film from compound **4** after thermal annealing (20 min at 100 °C).

10. NMR

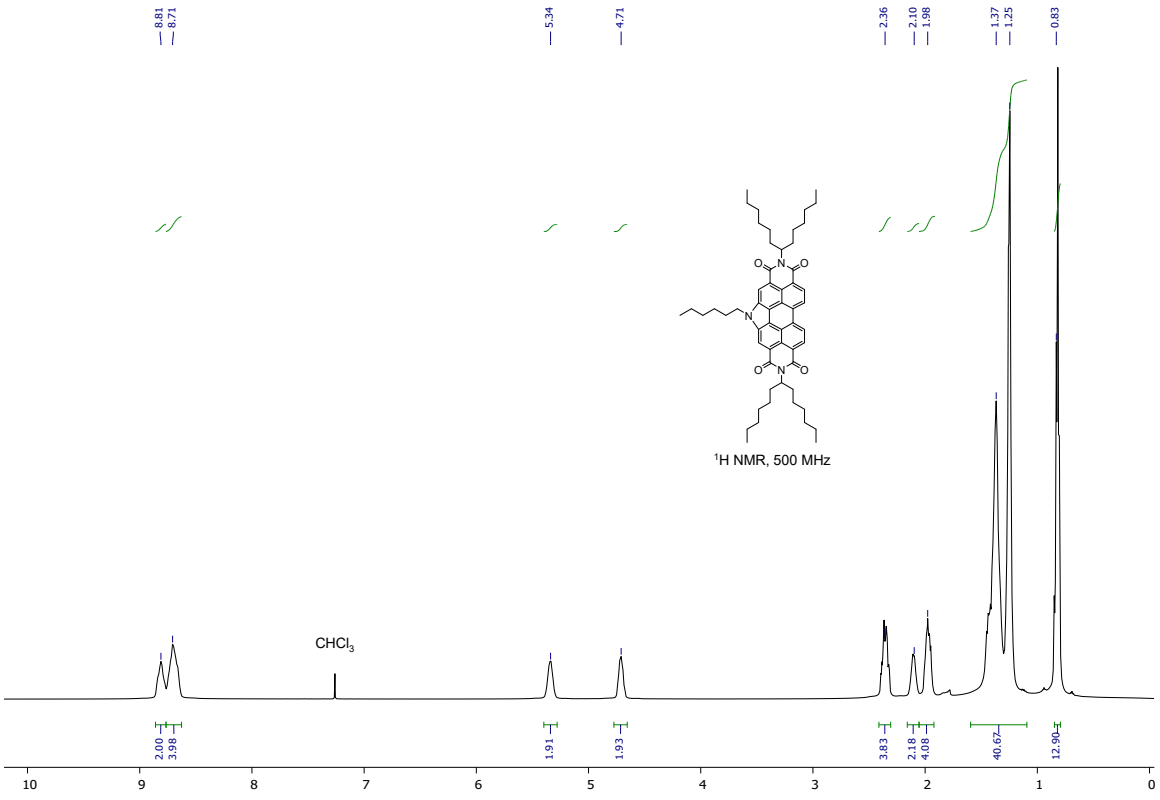

Figure S23. ^{1}H NMR spectrum of compound **6** in $CDCl_3$ at 298 K.

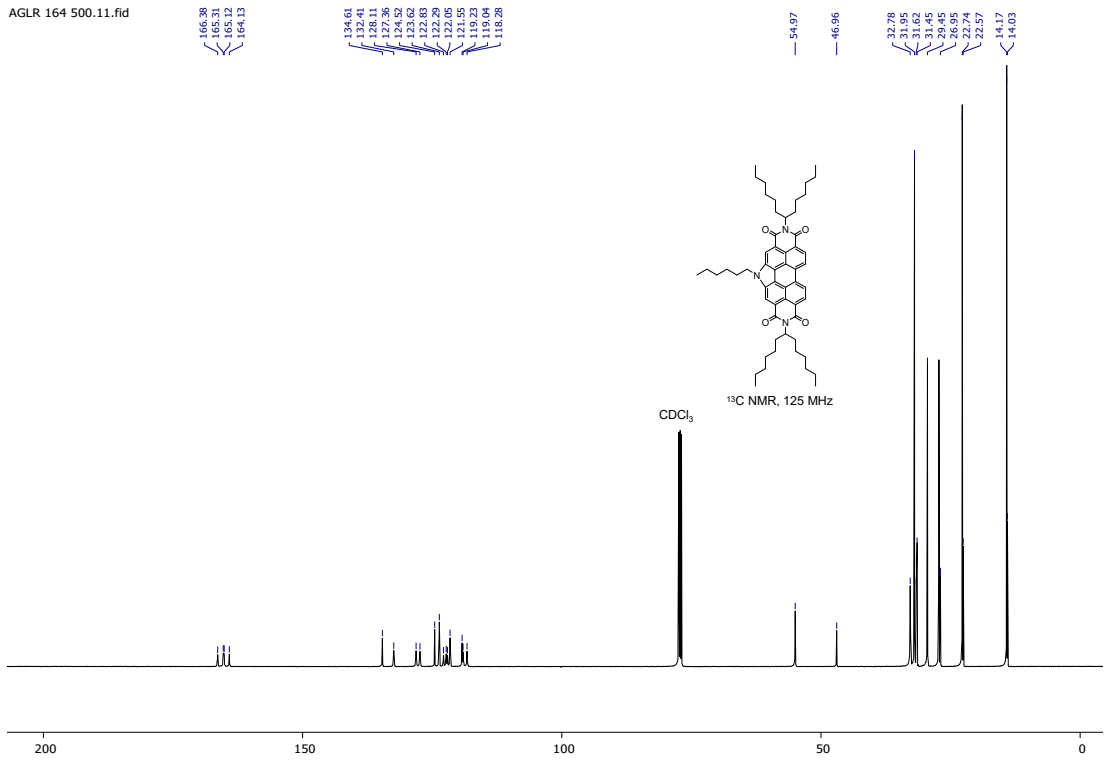

Figure S24. $^{13}C\{^{1}H\}$ NMR spectrum of compound **6** in $CDCl_3$ at 289 K.

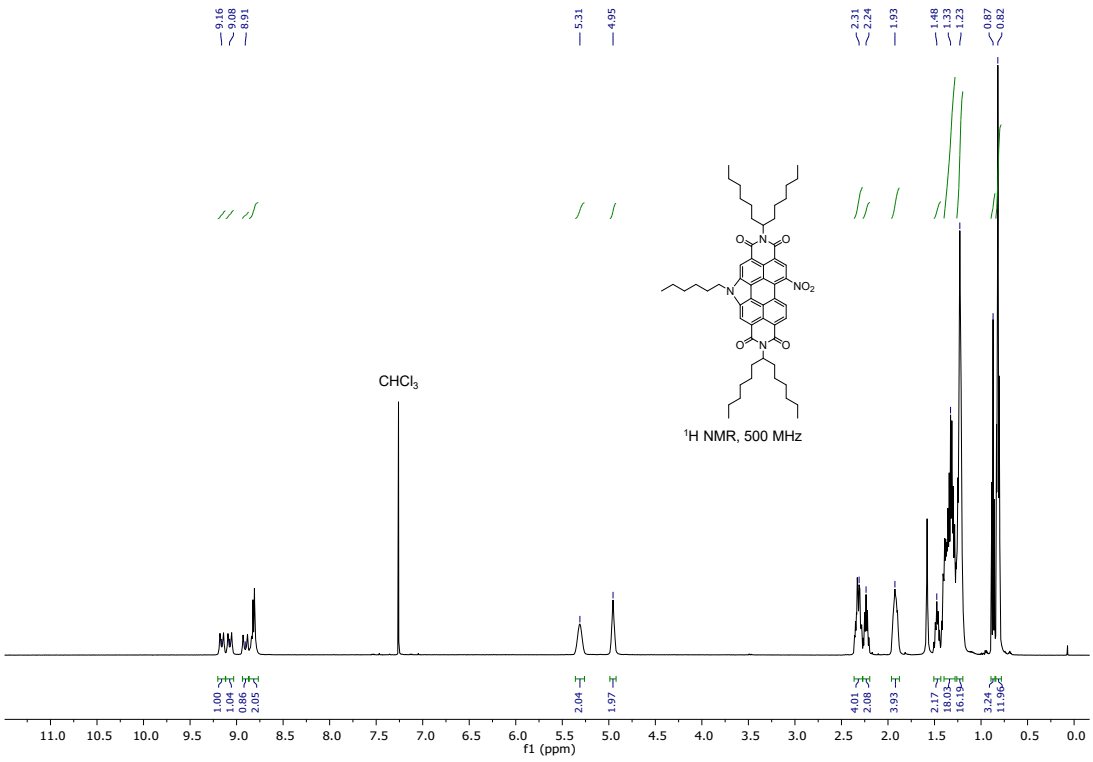

Figure S25. ^{1}H NMR spectrum of compound **7** in $CDCl_3$ at 298 K.

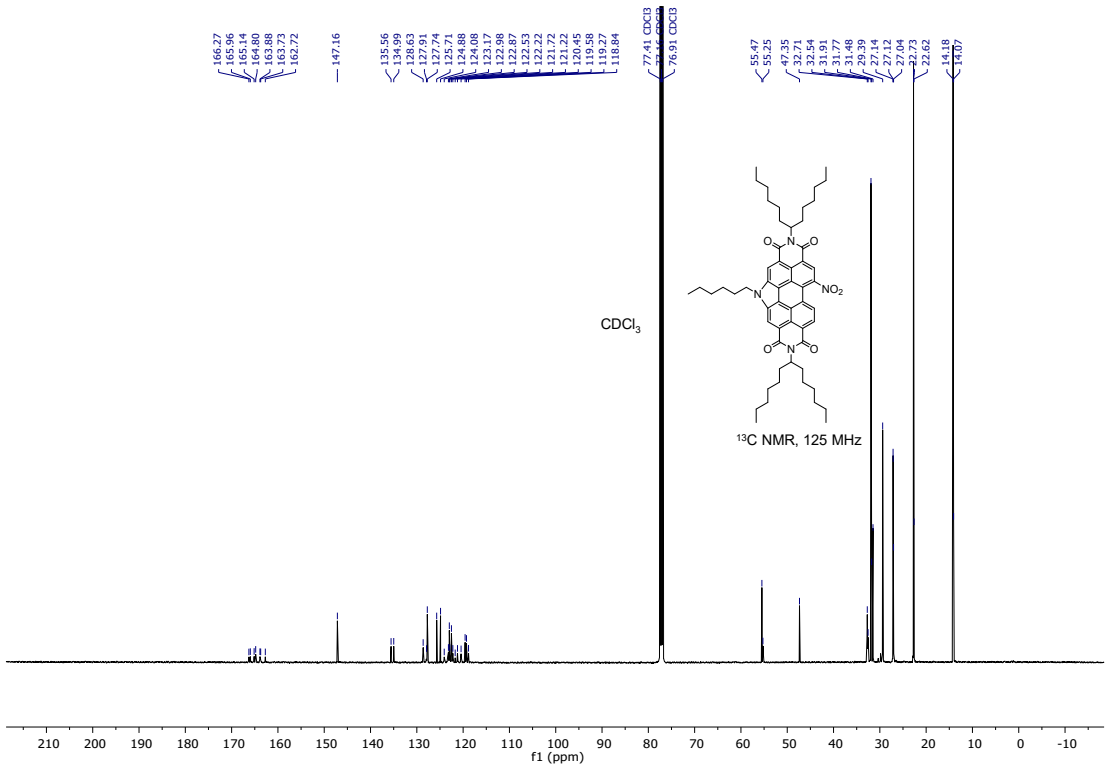

Figure S26. $^{13}C\{^{1}H\}$ NMR spectrum of compound **7** in $CDCl_3$ at 289 K.

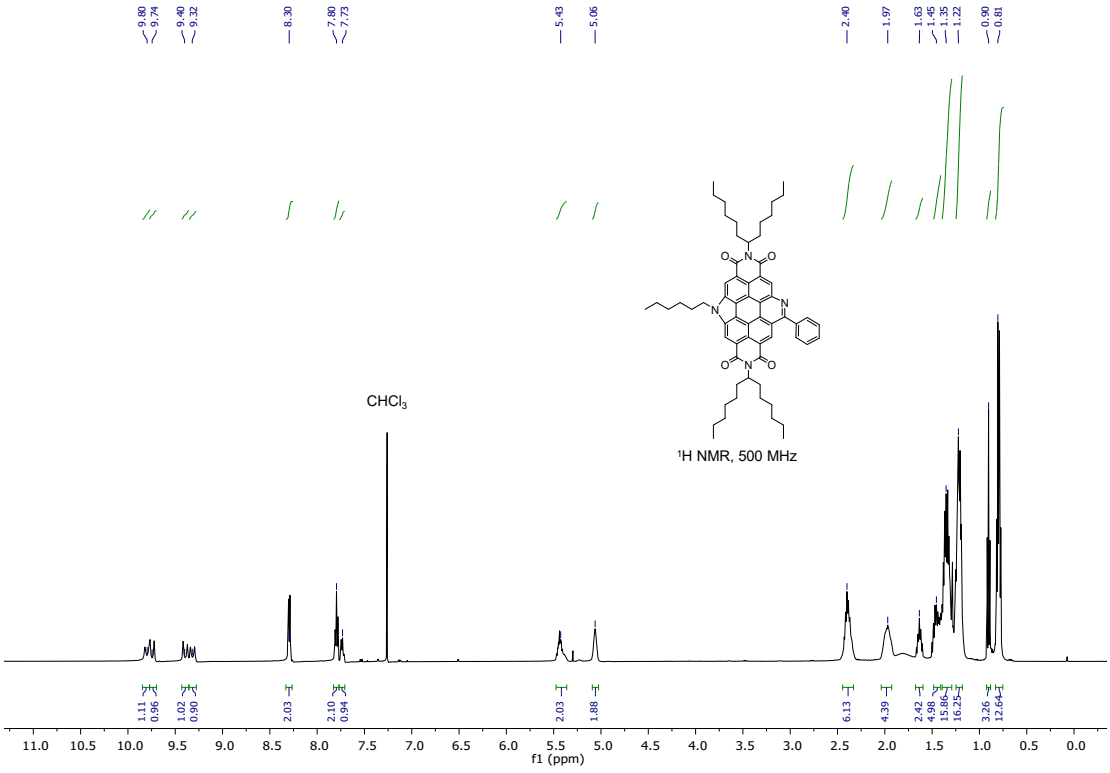

Figure S27. ^{1}H NMR spectrum of compound **2** in $CDCl_3$ at 298 K.

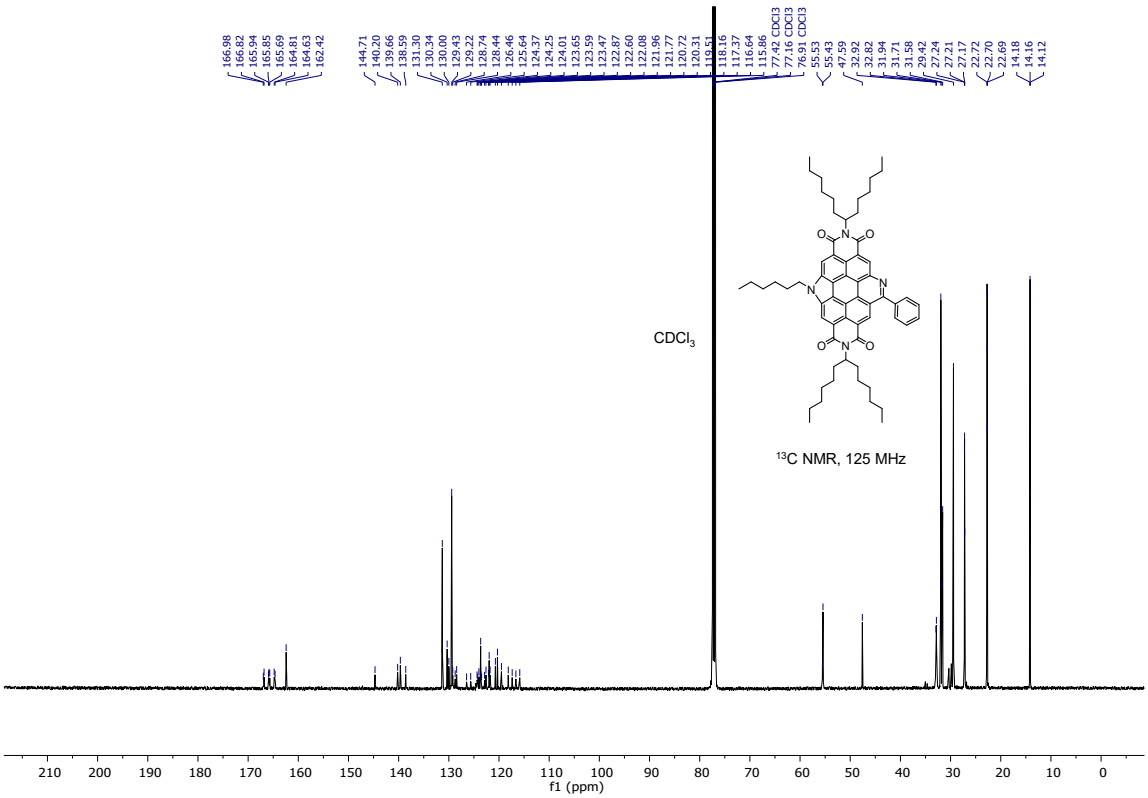

Figure S28. $^{13}C\{^{1}H\}$ NMR spectrum of compound **2** in $CDCl_3$ at 298 K.

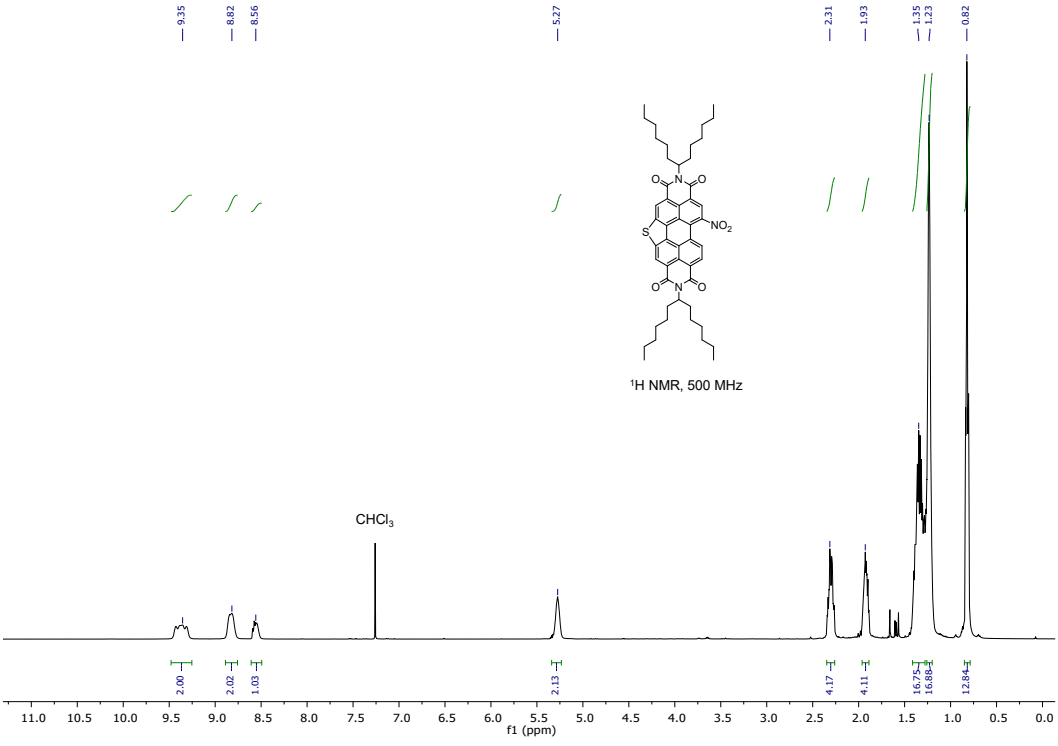

Figure S29. ^{1}H NMR spectrum of compound **12** in $CDCl_3$ at 298 K.

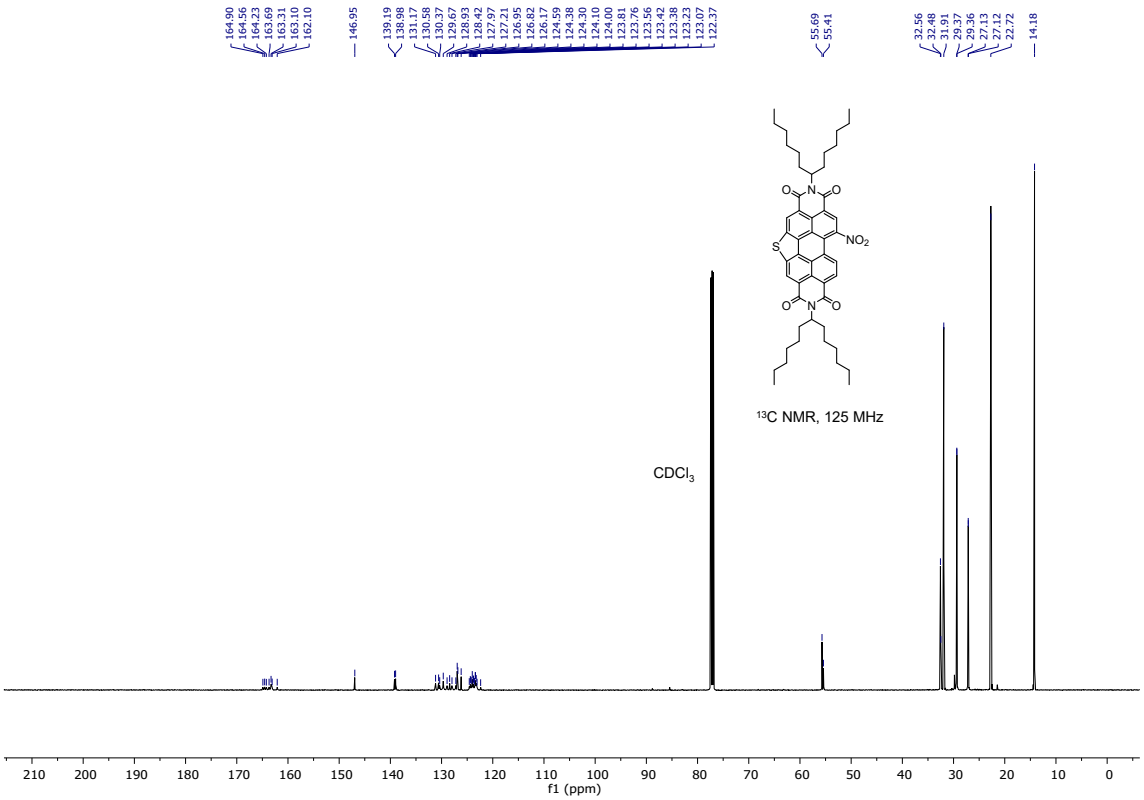

Figure S30. $^{13}C\{^{1}H\}$ NMR spectrum of compound **12** in $CDCl_3$ at 298 K.

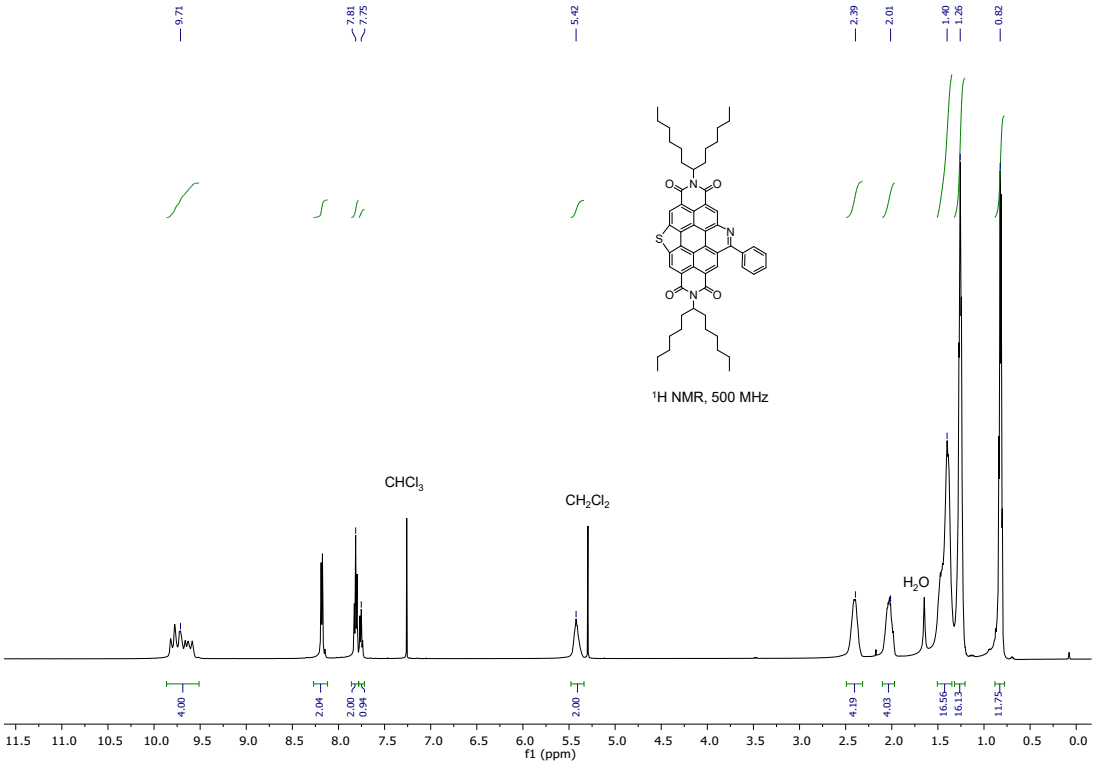

Figure S31. ^{1}H NMR spectrum of compound **3** in $CDCl_3$ at 298 K.

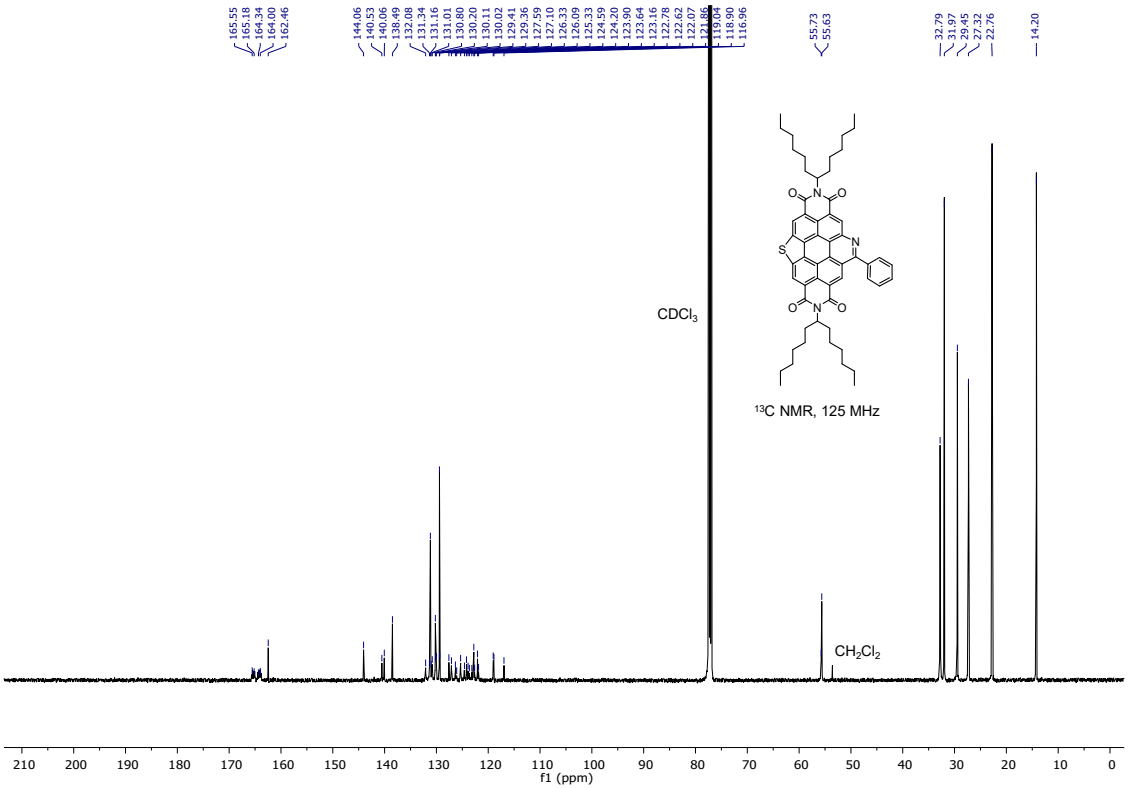

Figure S32. $^{13}C\{^{1}H\}$ NMR spectrum of compound **3** in $CDCl_3$ at 298K.

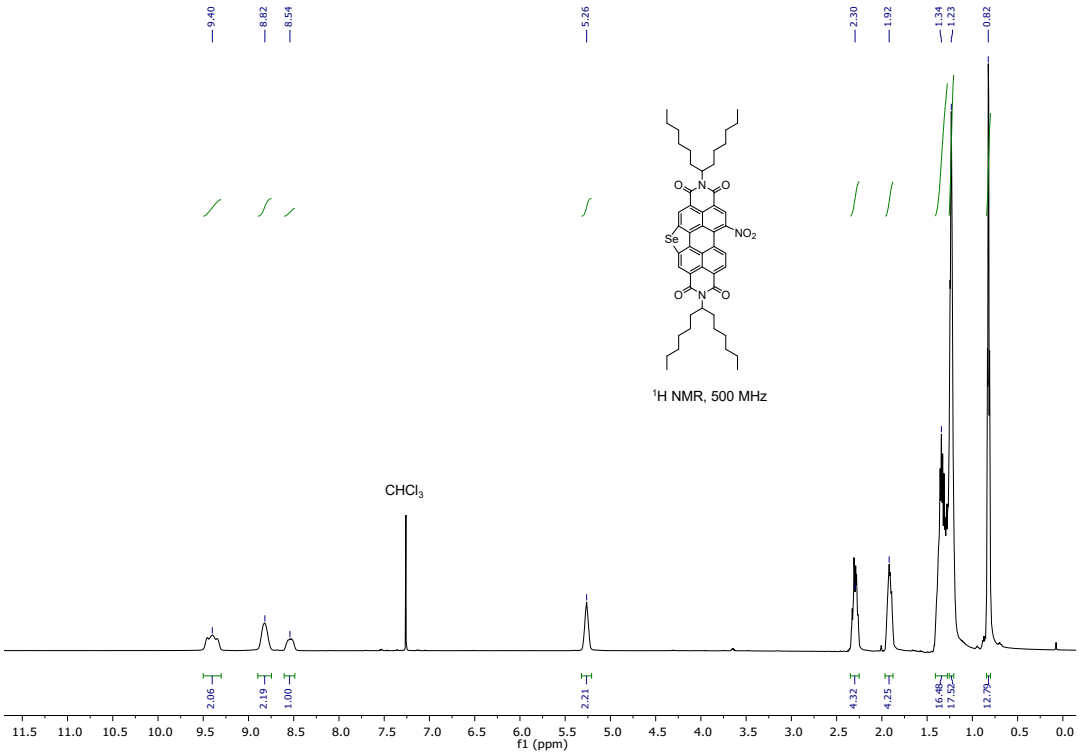

Figure S33. ^{1}H NMR spectrum of compound **13** in $CDCl_3$ at 298 K.

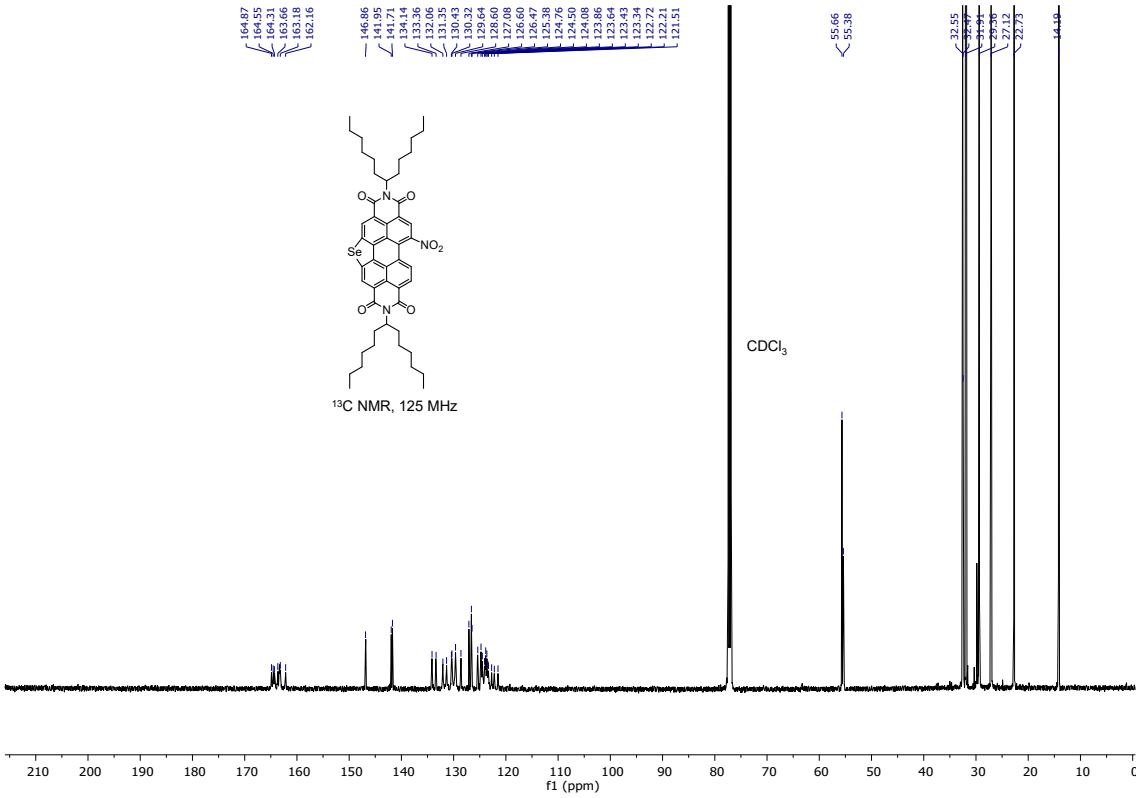

Figure S34. $^{13}C\{^{1}H\}$ NMR spectrum of compound **13** in $CDCl_3$ at 298 K.

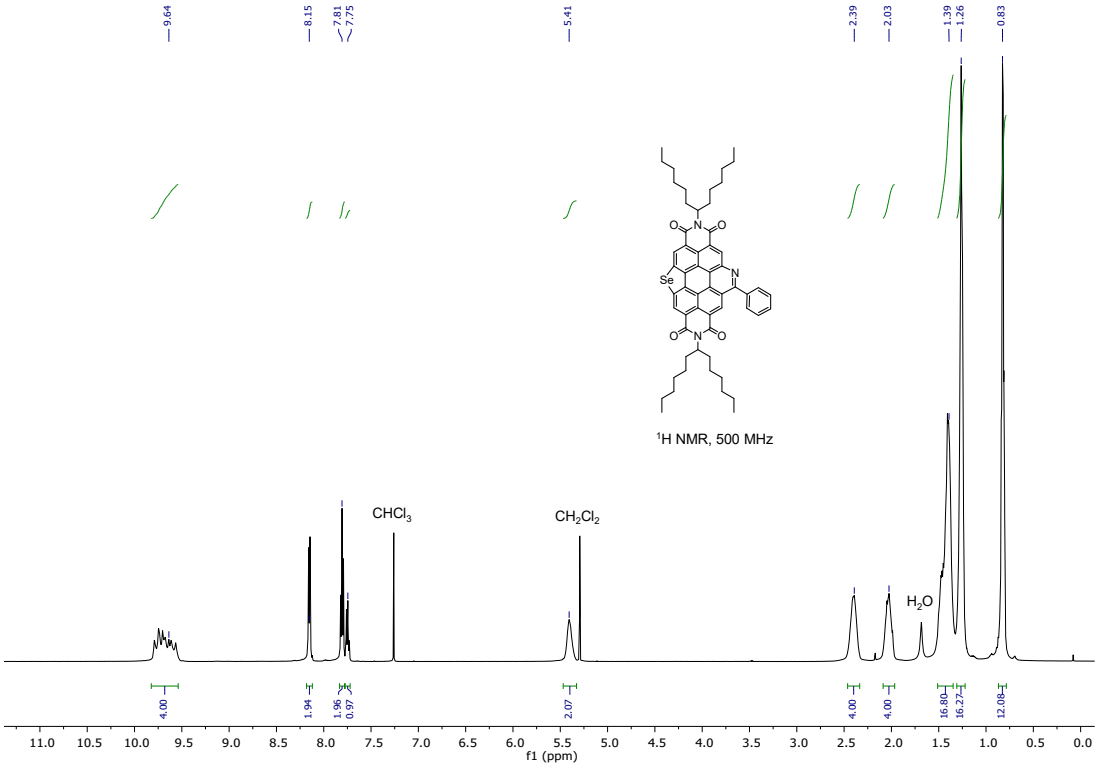

Figure S35. ^{1}H NMR spectrum of compound **4** in $CDCl_3$ at 298 K.

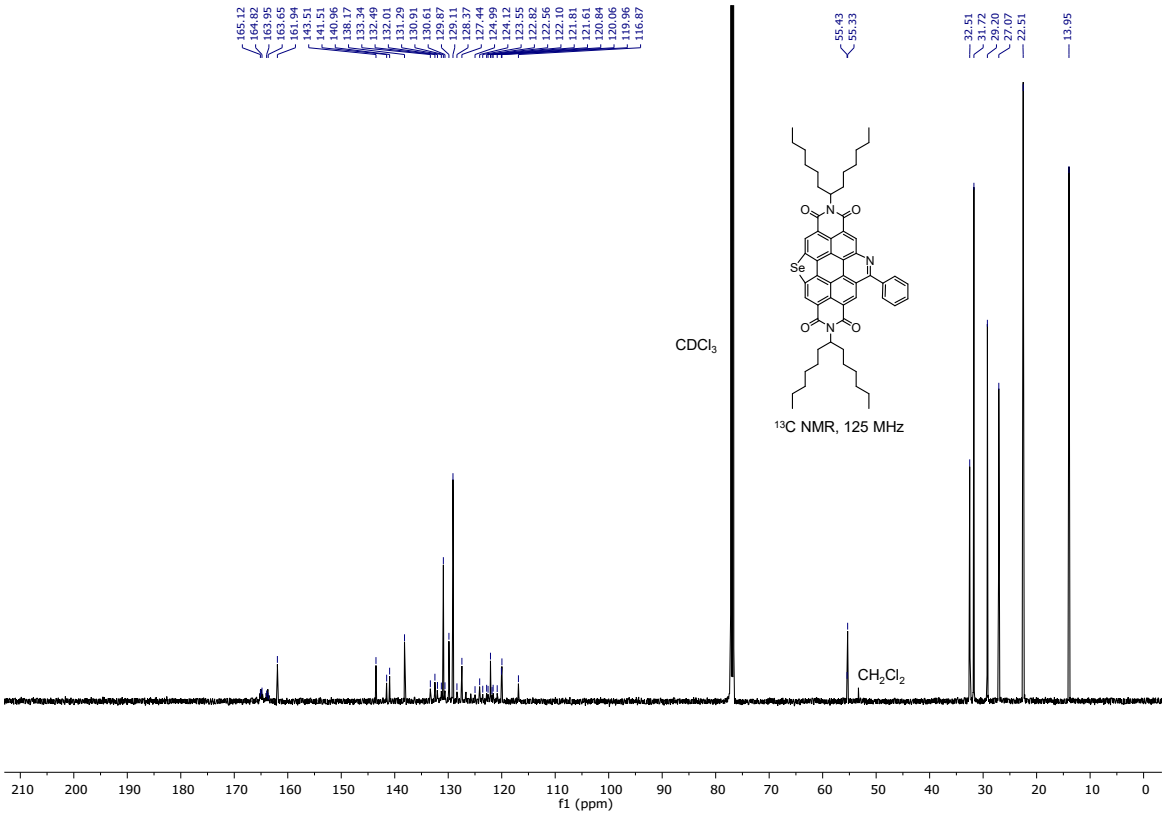

Figure S36. ^{1}H NMR spectrum of compound **4** in $CDCl_3$ at 298 K.

11. High Resolution Mass Spectrometry

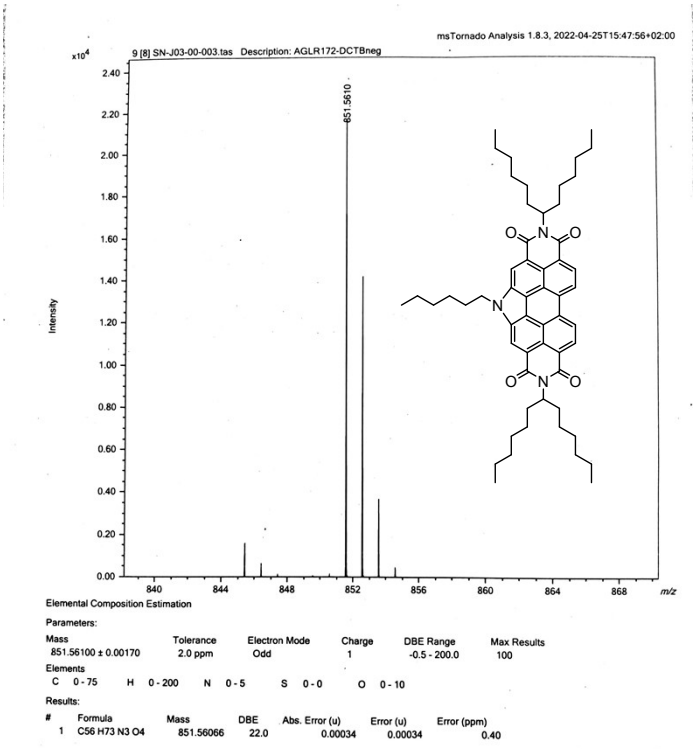

Figure S37. HRMS spectrum of compound **6**.

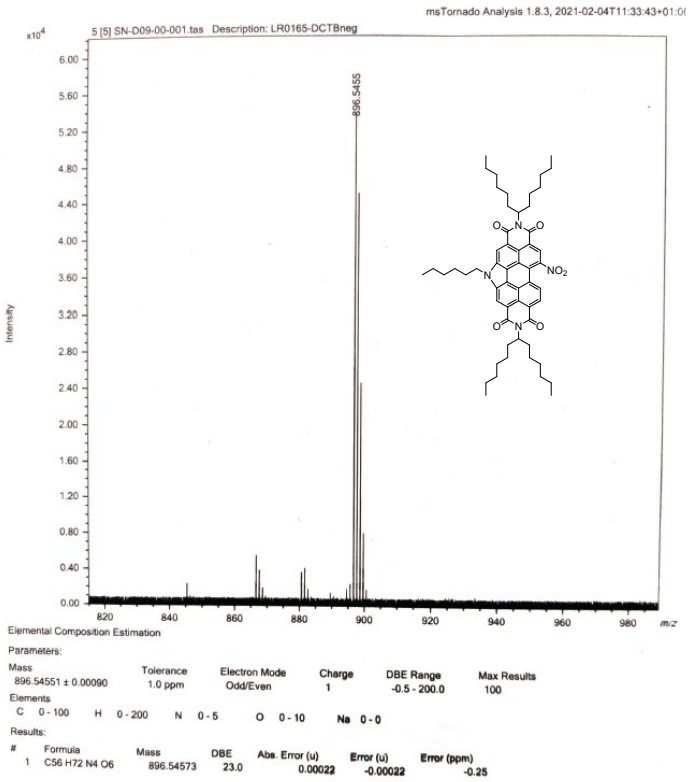

Figure S38. HRMS spectrum of compound **7**.

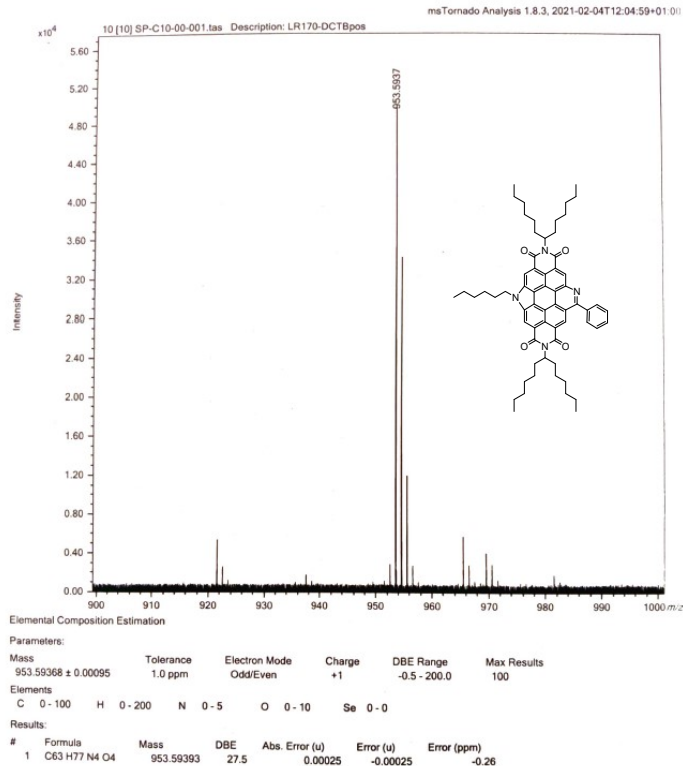

Figure S39. HRMS spectrum of compound **2**.

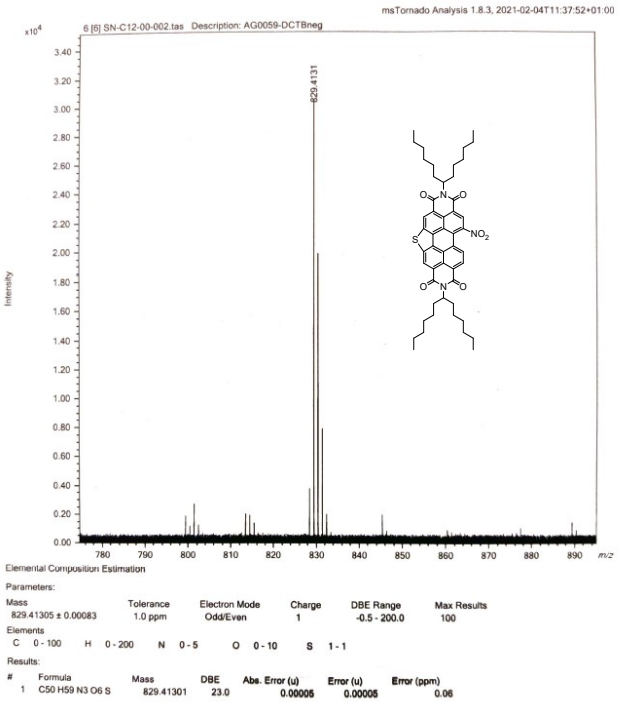

Figure S40. HRMS spectrum of compound **12**.

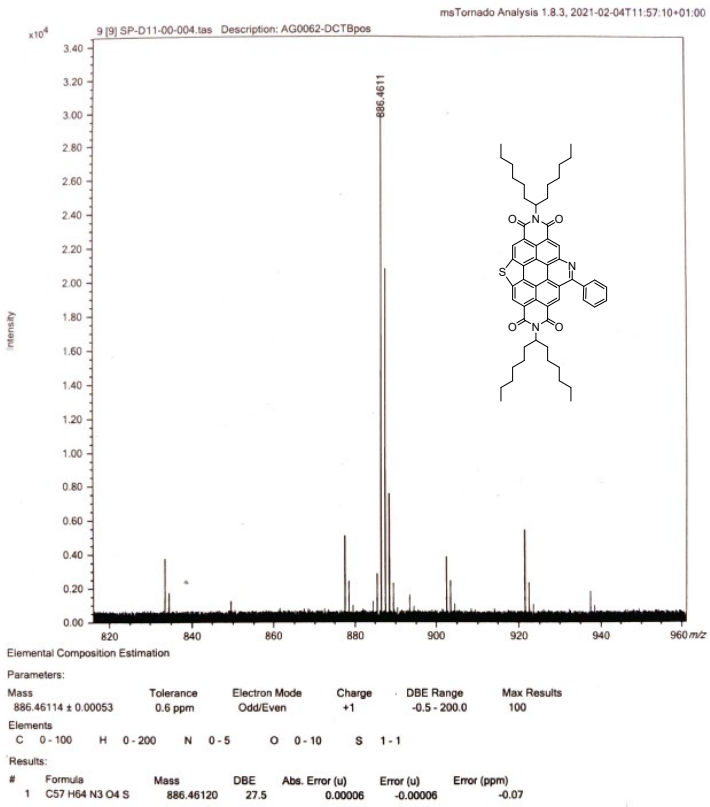

Figure S41. HRMS spectrum of compound **3**.

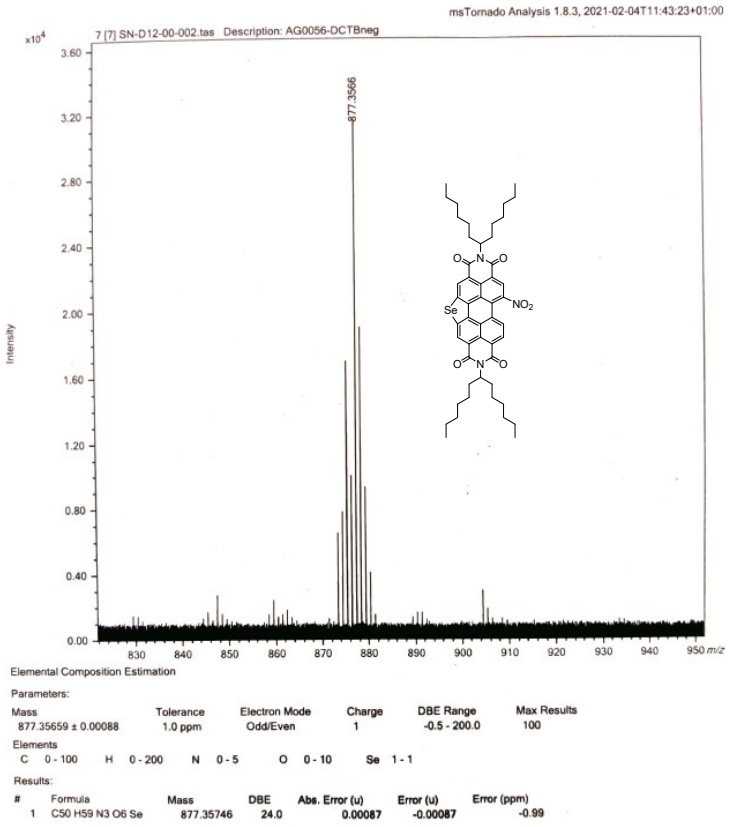

Figure S42. HRMS spectrum of compound **13**.

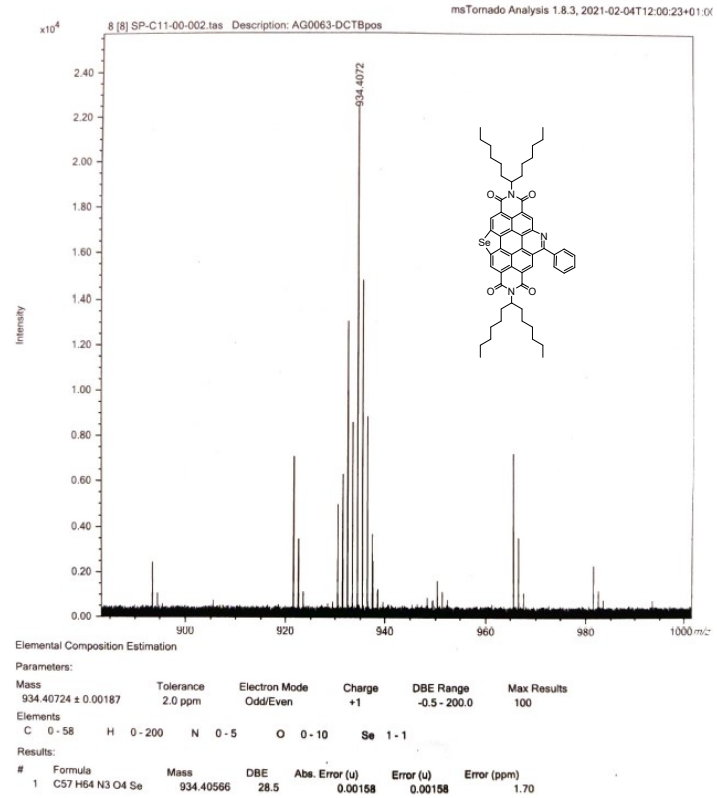

Figure S43. HRMS spectrum of compound **4**.

12. Calculations

Computational details

Software	Gaussian	(2009+D.01)
Computational method	DFT	
Functional	B3LYP	
Basis set name	6-31+G(2d,p)	
Number of basis set functions	1085	
Closed shell calculation	True	
Requested SCF convergence on RMS and Max density matrix	1e-08	1e-06
Requested SCF convergence on energy	1e-06	
Job type: Frequency and thermochemical analysis		
Temperature	298.15 K	
Job type: Time-dependent calculation		
Number of calculated excited states and spin state	15	['Singlet-A']

Compound 1

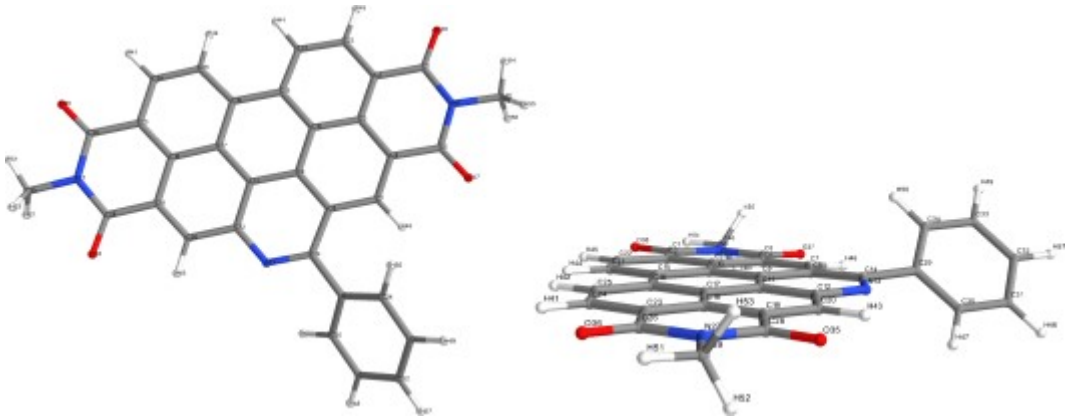

Figure S44. Chemical structure diagram with atomic numbering from two points of view.

Formula	C33H17N3O4
Charge	0
Spin multiplicity	1

Total molecular energy	-1733.20167 hartrees
HOMO number	134
LUMO+1 energies	-2.43 eV

LUMO energies	-3.63 eV
HOMO energies	-6.47 eV
HOMO-1 energies	-7.00 eV
Geometry optimization specific results	
Converged nuclear repulsion energy	4149.10702 Hartrees
Frequency and Thermochemistry specific results	
Enthalpy at 298.15 K	-1732.74916 Hartrees
Gibbs free energy at 298.15 K	-1732.83865 Hartrees
Entropy at 298.15 K	0.00030 Hartrees

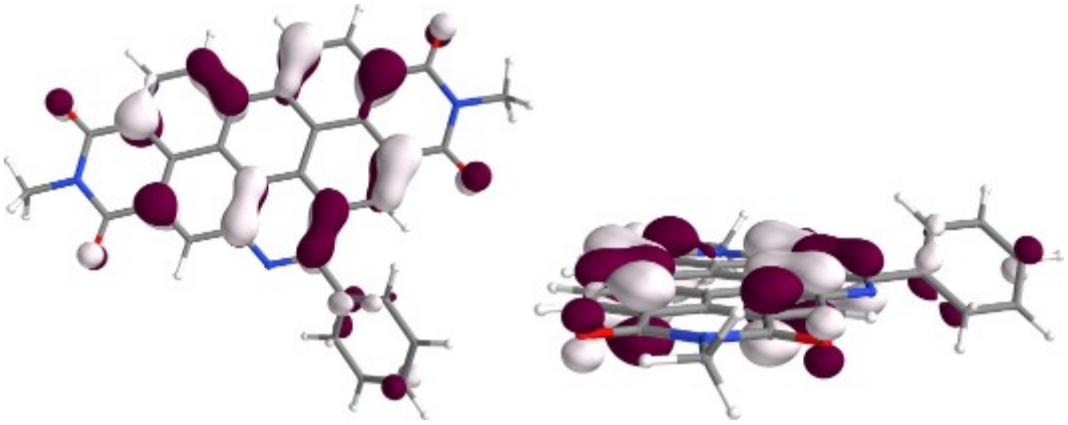

Figure S45. Representation of the HOMO from two points of view.

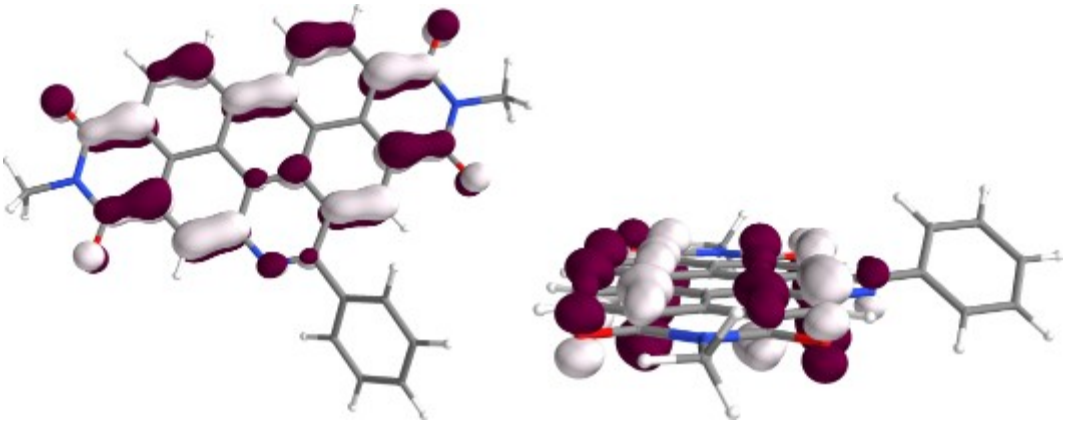

Figure S46. Representation of the LUMO from two points of view.

E.S.	Symmetry	nm	cm^{-1}	*f*	R	Λ	d_{CT}	q_{CT}	Excitation description : initial OM - ending OM (% if > 5%)
1	Singlet-A	478	20900	0.397	14.5	0.78	178.73	0.40	134-135(93);
2	Singlet-A	424	23531	0.146	-7.4	0.59	368.81	0.57	133-135(86); 134-136(6);
3	Singlet-A	385	25912	0.000	0.5	0.17	634.77	0.88	132-135(90);
4	Singlet-A	374	26696	0.000	1.2	0.32	546.86	0.81	130-135(90);

5	Singlet-A	370	26998	0.001	7.4	0.34	519.21	0.78	129-135(84);
6	Singlet-A	366	27294	0.045	-19.3	0.53	408.99	0.49	131-135(62); 134-136(20);
7	Singlet-A	356	28036	0.002	6.2	0.51	222.76	0.67	127-135(32); 128-135(57);
8	Singlet-A	351	28434	0.005	7.3	0.55	152.89	0.61	126-135(18); 127-135(55); 128-135(21);
9	Singlet-A	339	29473	0.113	-7.7	0.60	87.33	0.35	125-135(6); 131-135(19); 134-136(42);
10	Singlet-A	333	29944	0.046	13.6	0.58	66.66	0.33	126-135(30); 134-136(8); 134-138(40);
11	Singlet-A	331	30152	0.004	0.2	0.64	190.48	0.39	124-135(11); 125-135(13); 134-137(57);
12	Singlet-A	326	30662	0.010	-5.0	0.59	86.43	0.37	125-135(12); 126-135(24); 134-138(42);
13	Singlet-A	323	30907	0.000	3.6	0.31	599.07	0.78	123-135(87);
14	Singlet-A	319	31320	0.000	2.6	0.36	594.82	0.77	122-135(87);
15	Singlet-A	316	31625	0.327	14.1	0.52	130.05	0.47	125-135(53); 133-136(7); 134-136(9); 134-

Table S4. Results concerning the calculated mono-electronic excitations.

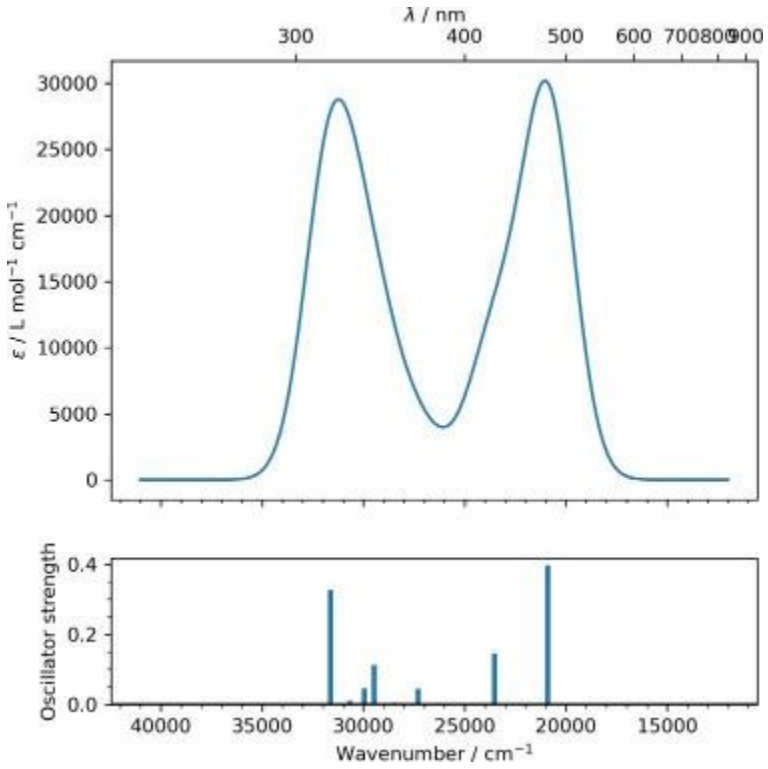

Figure S47. Calculated UV visible Absorption spectrum with a Gaussian broadening (FWHM = 3000 cm^{-1})

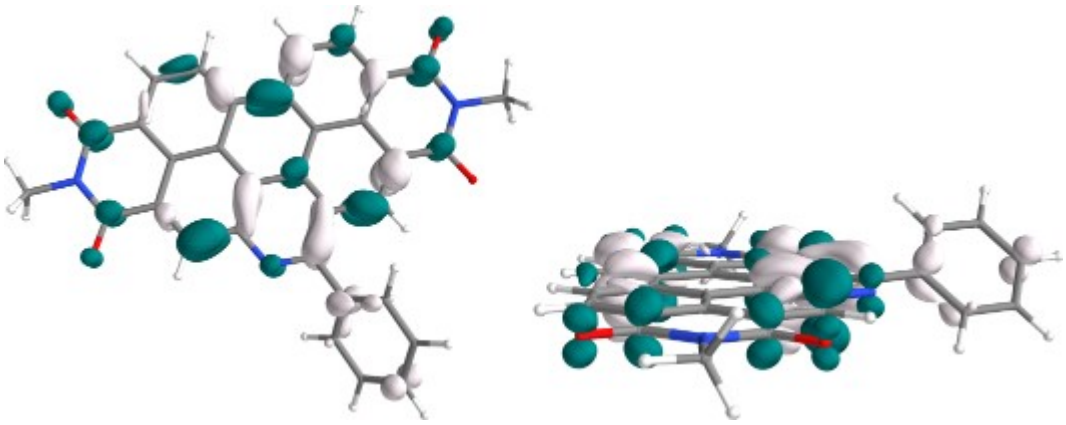

Figure S48. Representation of the Electron Density Difference (S1-S0) from two points of view.

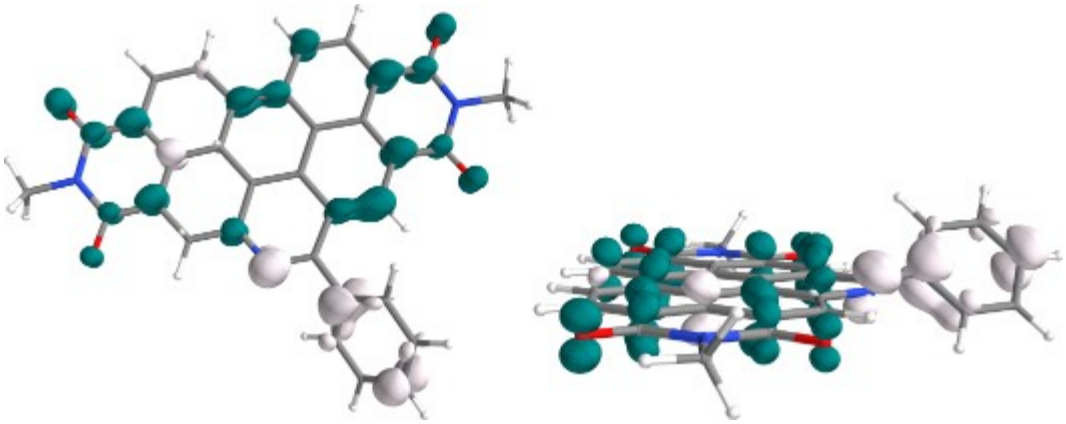

Figure S49. Representation of the Electron Density Difference (S2-S0) from two points of view.

E.S.	Symmetry	nm	cm^{-1}	*f*	R	Λ	d_{CT}	q_{CT}	Excitation description in %
2	Singlet-A	526	18979	0.374	26.267	0.79	181.02	0.40	133->135 (4) 134->135 (93)

Table S5. Results concerning the calculated mono-electronic optimization excitation

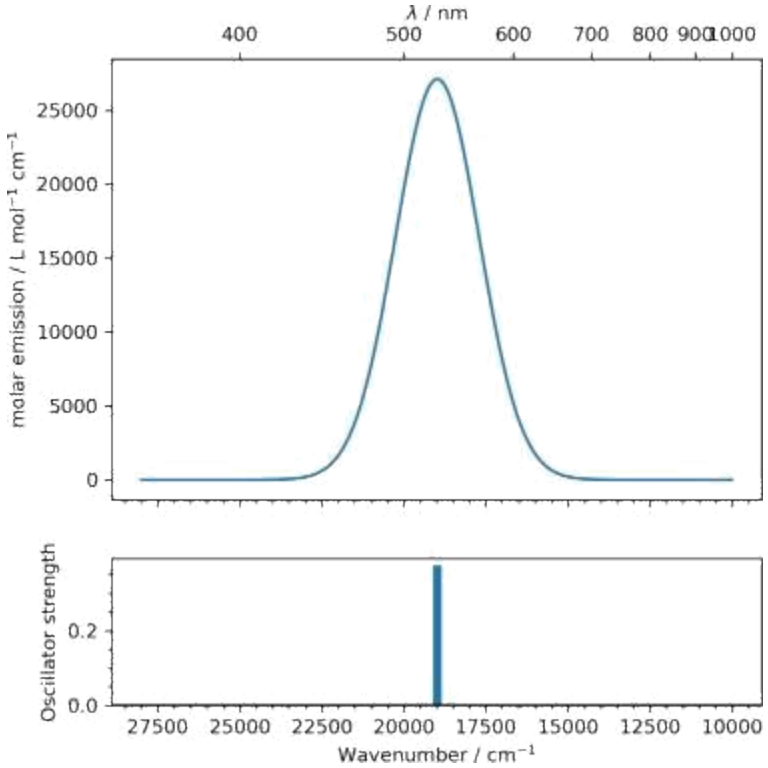

Figure S50. Calculated UV visible Emission spectrum with a Gaussian broadening (FWHM = 3000 cm^{-1})

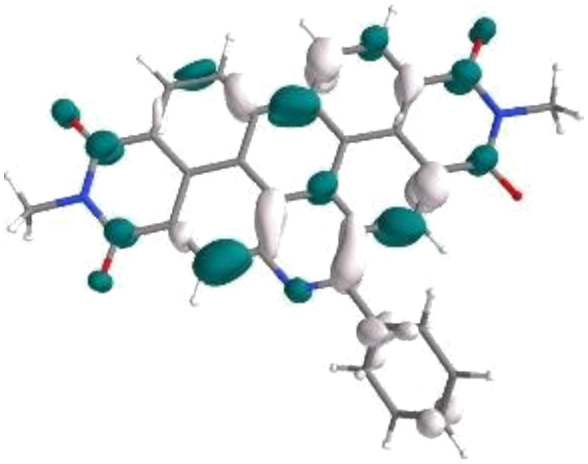

Figure S51. Representation of the Electron Density Difference (S1-GS) after optimization of the excited state. The excited electron and the hole regions are indicated by respectively white and blue surfaces to ease comparison with the corresponding absorption transition.

Atom	X	Y	Z
C	-4.2402	-3.2453	-0.0547
C	-2.7969	-2.9667	0.0131
C	-2.3149	-1.6383	-0.0189

C	-3.2159	-0.5515	-0.1232
C	-4.6683	-0.8013	-0.2057
N	-5.0903	-2.1300	-0.1638
C	-2.7546	0.7675	-0.1512
C	-1.3874	1.0557	-0.0468
C	-0.4616	-0.0356	0.0106
C	-0.9147	-1.3849	0.0368
C	0.9208	0.2304	0.0087
C	1.3629	1.5976	-0.0822
N	0.4784	2.6284	-0.1049
C	-0.8216	2.4002	-0.0371
C	0.0092	-2.4672	0.1078
C	1.4257	-2.1889	0.1216
C	1.8621	-0.8333	0.0525
C	3.2511	-0.5185	0.0228
C	3.6690	0.8428	-0.0722
C	2.7434	1.8743	-0.1285
C	-0.5208	-3.7867	0.1487
C	-1.8845	-4.0260	0.1051
C	4.1982	-1.5543	0.0824
C	3.7642	-2.8919	0.1673
C	2.4207	-3.2054	0.1841
C	5.6411	-1.2618	0.0563
N	6.0055	0.0900	-0.0396
C	5.1113	1.1626	-0.1105
C	-1.6523	3.6156	0.0689
C	-1.2428	4.7768	-0.6262
C	-1.9767	5.9496	-0.5385
C	-3.1174	6.0041	0.2709
C	-3.5167	4.8735	0.9922
C	-2.7990	3.6892	0.8884
O	5.5314	2.3087	-0.1986
O	6.4880	-2.1446	0.1132
O	-5.4861	0.1071	-0.3004
O	-4.6915	-4.3824	-0.0210
C	7.4312	0.4316	-0.0744
C	-6.5377	-2.3560	-0.2379
H	4.5180	-3.6694	0.2137
H	2.1311	-4.2468	0.2417

H	3.0807	2.9010	-0.1973
H	0.1499	-4.6343	0.2101
H	-2.2717	-5.0379	0.1337
H	-3.4924	1.5472	-0.2826
H	-0.3498	4.7248	-1.2366
H	-1.6631	6.8260	-1.0957
H	-4.3860	4.9204	1.6392
H	-3.0997	2.8321	1.4782
H	7.9982	-0.4936	-0.0090
H	7.6617	0.9597	-1.0024
H	7.6725	1.0920	0.7614
H	-6.7106	-3.4283	-0.1909
H	-7.0333	-1.8493	0.5932
H	-6.9285	-1.9434	-1.1706
H	-3.6878	6.9242	0.3459

Table S6. Converged cartesian atomic coordinates in Angstroms

Compound 2

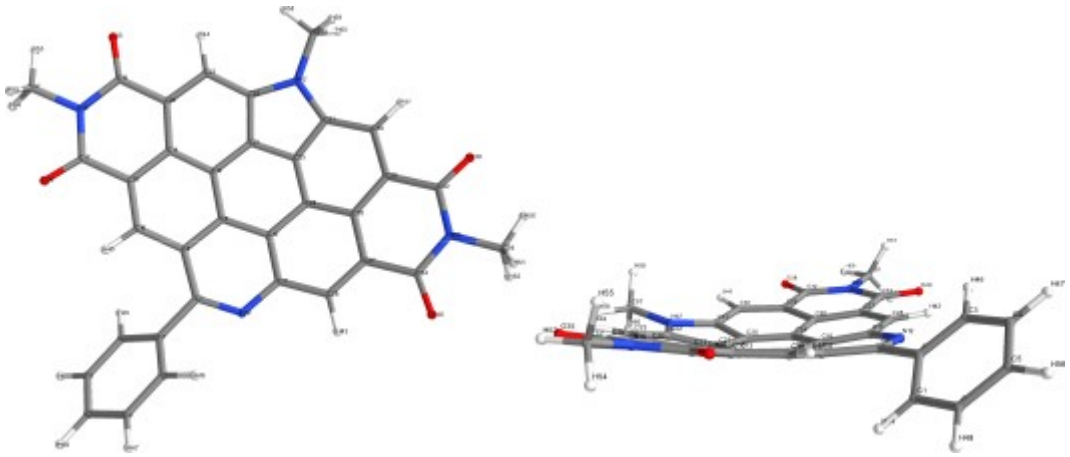

Figure S52. Chemical structure diagram with atomic numbering from two points of view.

Formula	C34H18N4O4	
Charge	0	
Spin multiplicity	1	
Total molecular energy		-1826.64372 hartrees
HOMO number		141
LUMO+1 energies		-2.43 eV

LUMO energies	-3.41 eV
HOMO energies	-6.31 eV
HOMO-1 energies	-6.55 eV
Geometry optimization specific results	
Converged nuclear repulsion energy	4562.02779 Hartrees
Frequency and Thermochemistry specific results	
Enthalpy at 298.15 K	-1826.16799 Hartrees
Gibbs free energy at 298.15 K	-1826.25915 Hartrees
Entropy at 298.15 K	0.00031 Hartrees

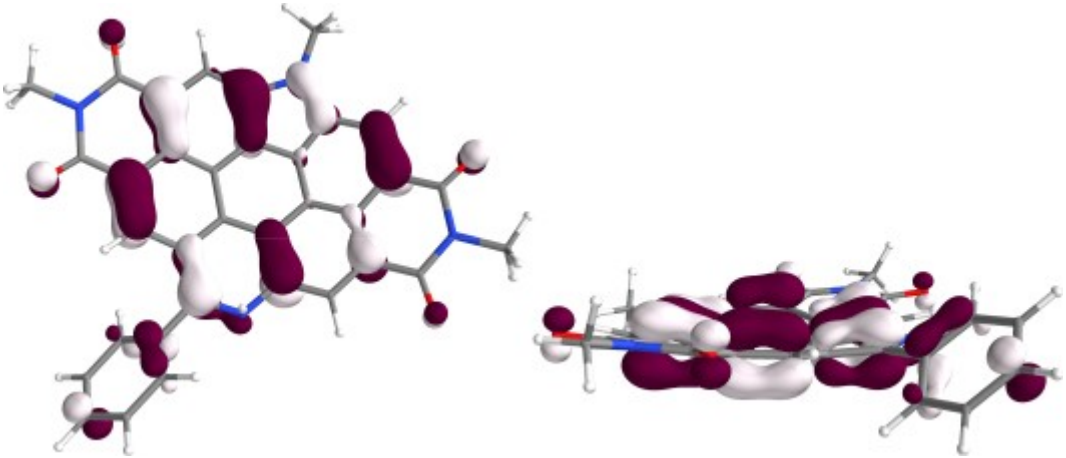

Figure S53. Representation of the HOMO from two points of view.

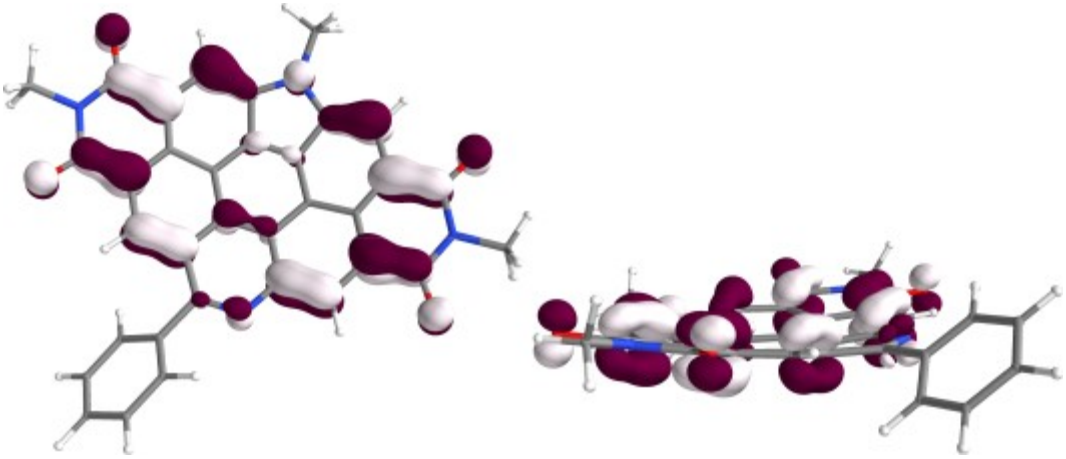

Figure S54. Representation of the LUMO from two points of view.

E.S.	Symmetry	nm	cm^{-1}	*f*	R	Λ	d_{CT}	q_{CT}	Excitation description : initial OM – ending OM (% if > 5%)
1	Singlet-A	481	20767	0.196	17.7	0.76	132.95	0.40	140-142(13); 141-142(79);
2	Singlet-A	447	22323	0.254	-1.2	0.73	92.46	0.43	140-142(75); 141-142(14); 141-

									143(7);
3	Singlet-A	378	26391	0.017	-1.9	0.39	572.28	0.75	139-142(94);
4	Singlet-A	366	27254	0.001	-6.3	0.31	373.15	0.78	137-142(59); 138-142(33);
5	Singlet-A	364	27469	0.001	-6.6	0.28	427.11	0.79	136-142(10); 137-142(27); 138-142(52);
6	Singlet-A	360	27739	0.001	6.4	0.35	427.26	0.78	136-142(79); 138-142(6);
7	Singlet-A	355	28152	0.418	37.5	0.66	275.14	0.46	140-142(6); 141-143(82);
8	Singlet-A	344	28994	0.002	-2.4	0.42	246.70	0.62	134-142(44); 135-142(43);
9	Singlet-A	344	29046	0.003	7.6	0.43	266.23	0.66	134-142(42); 135-142(45);
10	Singlet-A	340	29402	0.010	-16.9	0.65	167.26	0.50	141-144(63); 141-145(28);
11	Singlet-A	335	29828	0.140	41.3	0.62	305.21	0.35	140-143(48); 141-144(6); 141-145(20);
12	Singlet-A	332	30111	0.133	21.5	0.61	65.17	0.34	132-142(6); 140-143(25); 141-144(16); 141-
									145(40);
13	Singlet-A	323	30899	0.010	-10.7	0.58	180.12	0.44	131-142(7); 133-142(28); 140-144(47);

Table S7. Results concerning the calculated mono-electronic excitations.

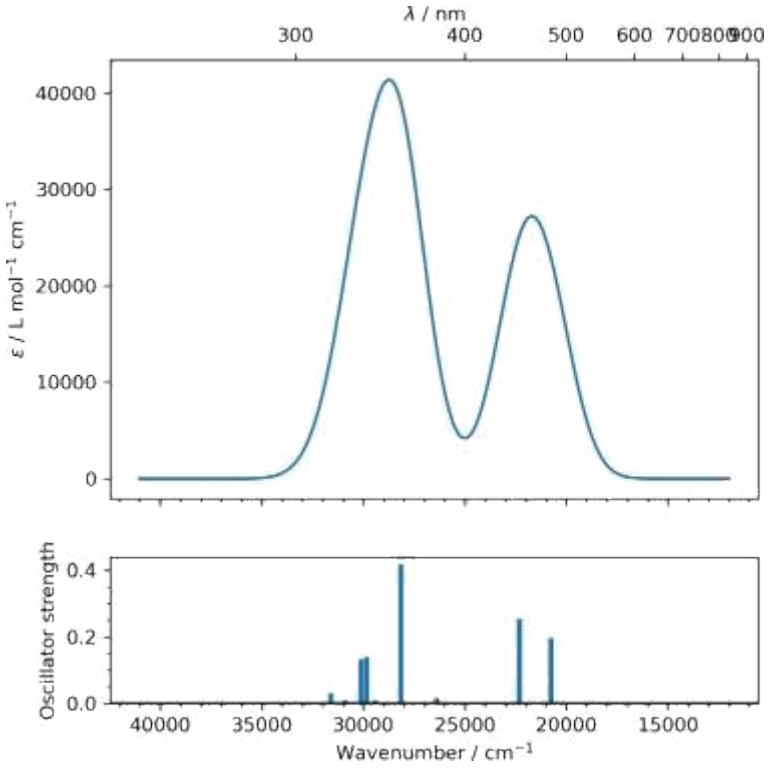

Figure S55. Calculated UV visible Absorption spectrum with a Gaussian broadening (FWHM = 3000 cm^{-1})

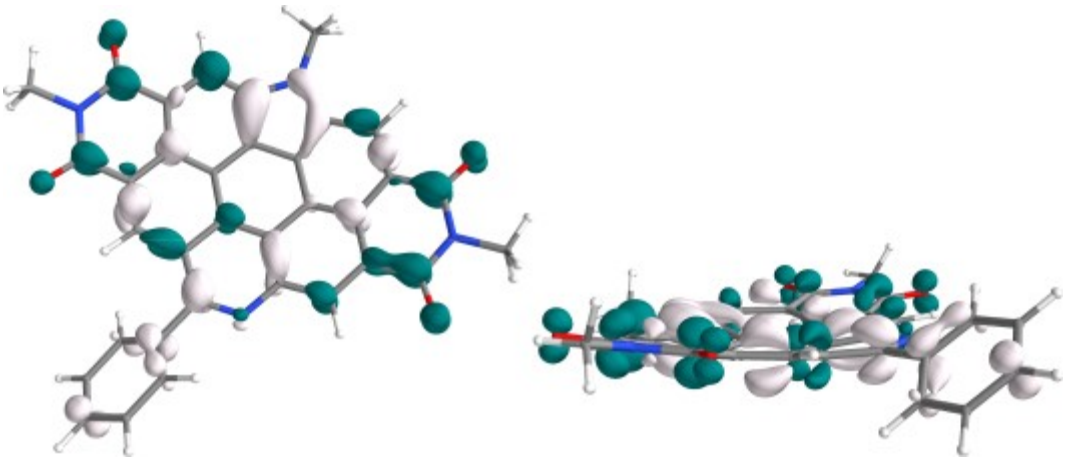

Figure S56. Representation of the Electron Density Difference (S1-S0) from two points of view.

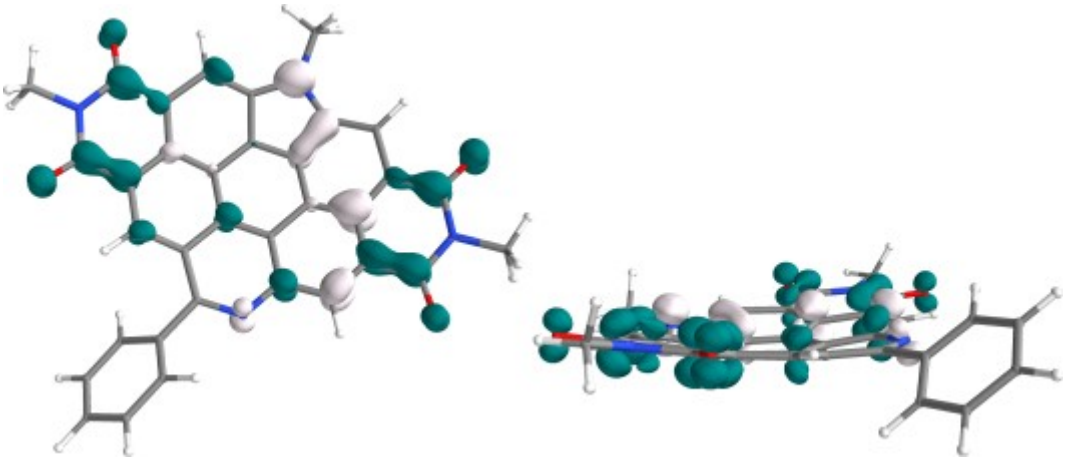

Figure S57. Representation of the Electron Density Difference (S2-S0) from two points of view.

E.S.	Symmetry	nm	cm^{-1}	*f*	R	Λ	d_{CT}	q_{CT}	Excitation description in %
2	Singlet-A	523	19112	0.243	32.0152	0.77	158.62	0.42	140->142 (5) 140->143 (2) 141->142

Table S8. Results concerning the calculated mono-electronic optimization excitation

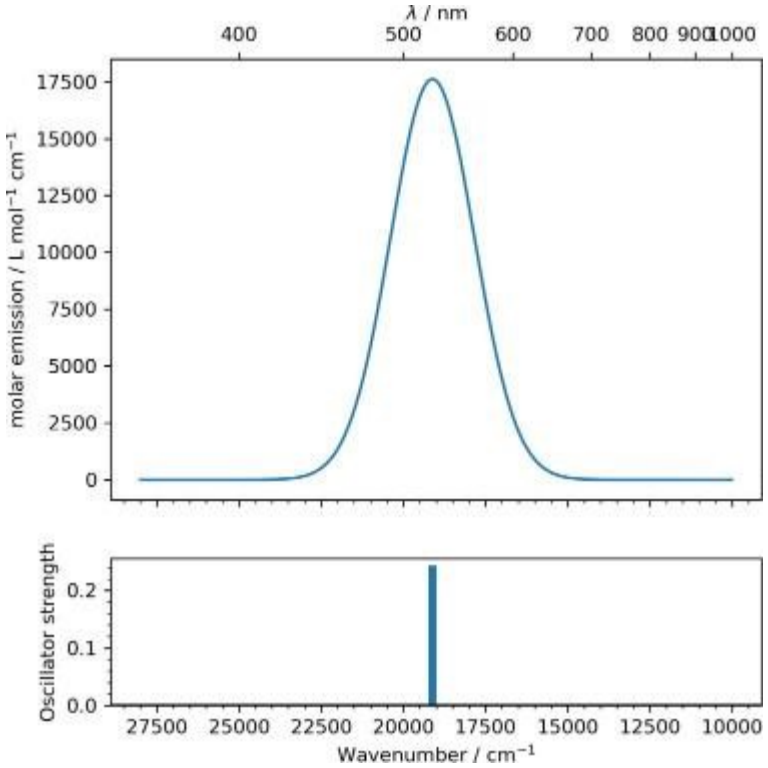

Figure S58. Calculated UV visible Emission spectrum with a Gaussian broadening (FWHM = 3000 cm-1)

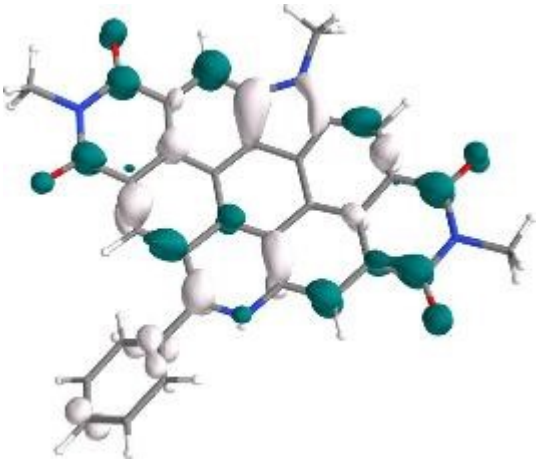

Figure S59. Representation of the Electron Density Difference (S1-GS) after optimization of the excited state. The excited electron and the hole regions are indicated by respectively white and blue surfaces to ease comparison with the corresponding absorption transition.

Atom	X	Y	Z
C	3.4598	3.6798	-0.8032
C	2.2425	3.7505	-0.0940
C	1.9354	4.9405	0.6029
C	2.8299	6.0006	0.6197
C	4.0382	5.9118	-0.0803

C	4.3435	4.7521	-0.7991
C	1.2672	2.6467	-0.1014
C	1.6767	1.2418	-0.1821
C	0.6125	0.3299	-0.4315
C	-0.7309	0.7737	-0.4457
C	-1.0274	2.1394	-0.1652
N	-0.0111	3.0314	-0.0353
C	0.8854	-1.0590	-0.4816
C	2.1440	-1.6133	-0.1995
C	3.1985	-0.7068	0.0426
C	2.9582	0.6878	0.0511
C	4.5238	-1.2594	0.3514
N	4.6202	-2.6631	0.3972
C	3.5670	-3.5933	0.2430
C	2.2393	-3.0363	-0.0643
C	-0.1759	-1.9338	-0.5978
C	-0.1535	-3.3252	-0.3625
C	1.1116	-3.8993	-0.1236
C	-1.7911	-0.1537	-0.5124
C	-1.4786	-1.4962	-0.6155
C	-3.1329	0.1788	-0.2449
C	-3.4270	1.5595	-0.0124
C	-2.3994	2.5053	0.0151
C	-4.0616	-0.8789	-0.1174
C	-3.6813	-2.2685	-0.1596
C	-2.3399	-2.5771	-0.3896
C	-5.4616	-0.5232	0.1644
N	-5.7482	0.8517	0.2993
C	-4.8270	1.9193	0.2576
O	3.7658	-4.7963	0.3659
O	5.5131	-0.5658	0.5578
C	5.9582	-3.1928	0.6861
O	-6.3427	-1.3683	0.2786
C	-7.1403	1.2362	0.5594
O	-5.2102	3.0667	0.4437
H	-4.4553	-2.9998	0.0427
N	-1.4954	-3.7288	-0.2975
H	-2.6453	3.5414	0.2193
H	1.2762	-4.9528	0.0692

H	3.7988	1.3184	0.3135
H	0.9933	5.0001	1.1333
H	2.5895	6.9002	1.1765
H	5.2689	4.6881	-1.3616
H	3.6918	2.8004	-1.3913
H	-7.7534	0.3406	0.5014
H	-7.2241	1.6902	1.5501
H	-7.4576	1.9751	-0.1788
H	5.9181	-4.2751	0.5939
H	6.6765	-2.7664	-0.0163
H	6.2639	-2.9114	1.6973
H	4.7344	6.7443	-0.0721
C	-1.9628	-5.0659	0.0141
H	-1.1747	-5.7864	-0.2106
H	-2.2352	-5.1553	1.0729
H	-2.8368	-5.3058	-0.5976

Table S9. Converged cartesian atomic coordinates in Angstroms

Compound 3

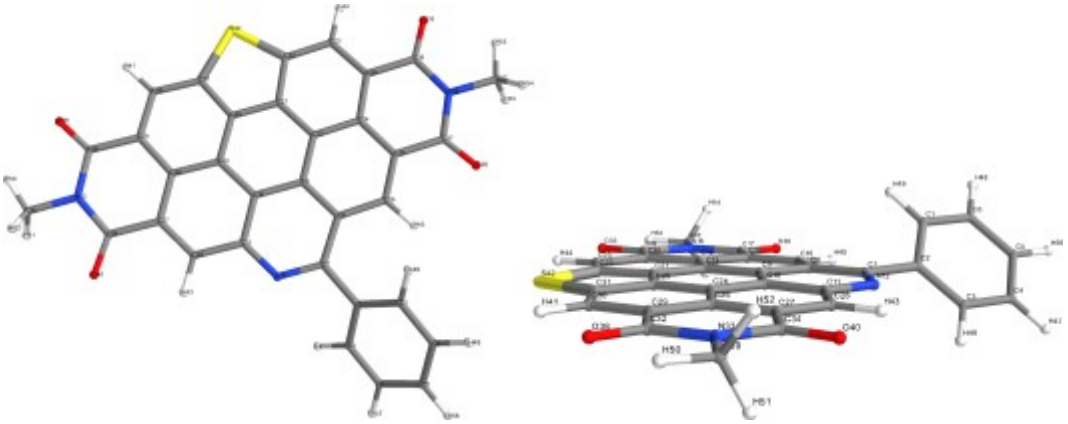

Figure S60. Chemical structure diagram with atomic numbering from two points of view.

Formula	C33H15N3O4S	
Charge	0	
Spin multiplicity	1	
Total molecular energy		-2130.18582 hartrees
HOMO number		141
LUMO+1 energies		-2.60 eV

LUMO energies	-3.62 eV
HOMO energies	-6.57 eV
HOMO-1 energies	-6.84 eV

Geometry optimization specific results

Converged nuclear repulsion energy	4538.28328 Hartrees

Frequency and Thermochemistry specific results

Enthalpy at 298.15 K	-2129.75311 Hartrees
Gibbs free energy at 298.15 K	-2129.84270 Hartrees
Entropy at 298.15 K	0.00030 Hartrees

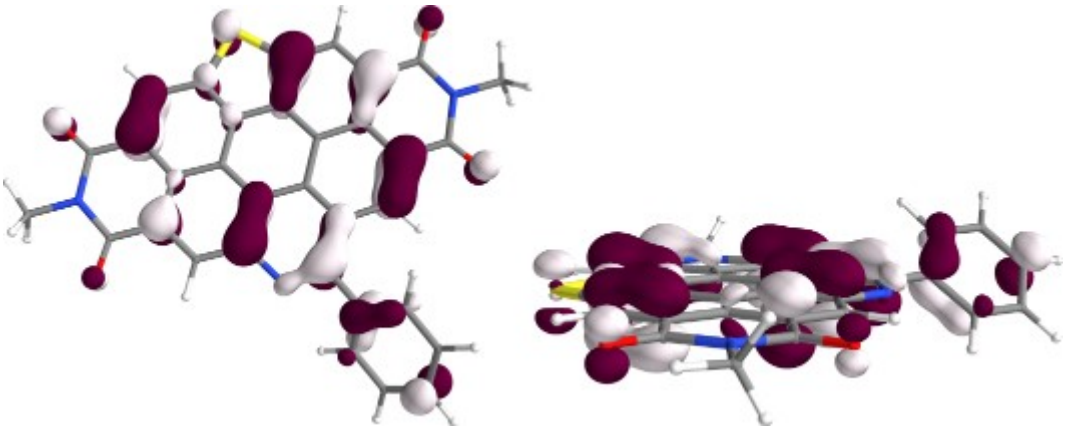

Figure S61. Representation of the HOMO from two points of view.

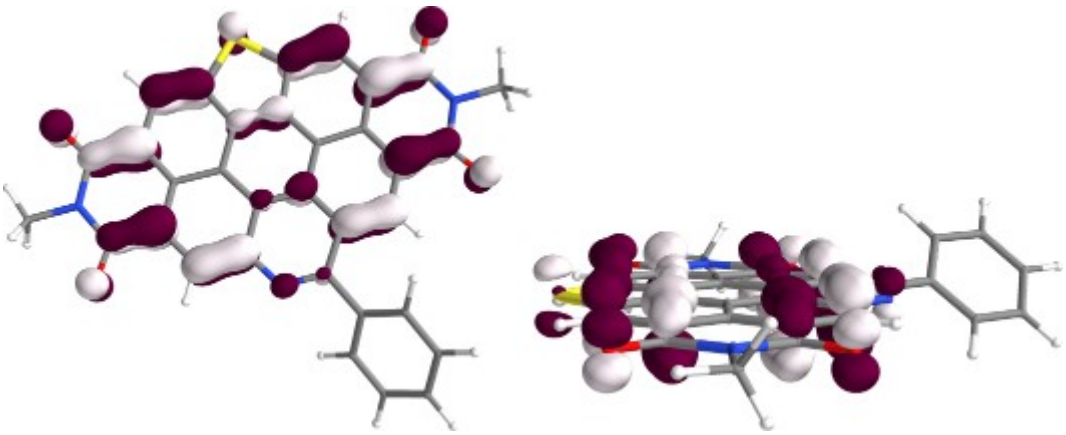

Figure S62. Representation of the LUMO from two points of view.

E.S.	Symmetry	nm	cm^{-1}	*f*	R	Λ	d_{CT}	q_{CT}	Excitation description : initial OM - ending OM (% if > 5%)
1	Singlet-A	472	21165	0.216	11.0	0.75	178.39	0.40	140-142(10); 141-142(83);
2	Singlet-A	437	22877	0.239	1.1	0.72	89.13	0.44	140-142(78); 141-142(11); 141-143(7);
3	Singlet-A	385	25928	0.024	-2.1	0.35	592.98	0.80	139-142(93);

4	Singlet-A	373	26748	0.014	-2.3	0.31	586.96	0.81	137-142(7); 138-142(88);
5	Singlet-A	371	26952	0.001	-2.5	0.32	521.98	0.80	137-142(83); 138-142(7);
6	Singlet-A	366	27309	0.000	0.3	0.33	548.02	0.80	136-142(89);
7	Singlet-A	351	28471	0.000	4.3	0.47	265.80	0.69	134-142(54); 135-142(37);
8	Singlet-A	348	28710	0.386	19.0	0.64	198.38	0.45	140-142(6); 141-143(77);
9	Singlet-A	345	28962	0.007	-4.6	0.52	212.52	0.63	132-142(10); 134-142(35); 135-142(46);
10	Singlet-A	330	30214	0.006	0.6	0.65	205.96	0.47	131-142(10); 141-144(62); 141-145(21);
11	Singlet-A	328	30441	0.025	7.3	0.59	161.41	0.32	132-142(22); 140-143(6); 141-144(9); 141-145(46);
12	Singlet-A	324	30772	0.223	36.3	0.58	350.07	0.41	133-142(12); 140-143(61);
13	Singlet-A	322	31015	0.037	-0.5	0.50	105.36	0.47	130-142(14); 131-142(9); 132-142(11); 133-142(36); 140-144(11);
14	Singlet-A	320	31204	0.011	2.2	0.32	549.66	0.73	130-142(74); 133-142(9);
15	Singlet-A	317	31532	0.063	19.8	0.53	187.40	0.36	132-142(29); 133-142(21); 140-143(6); 141-145(18);

Table S10. Results concerning the calculated mono-electronic excitations.

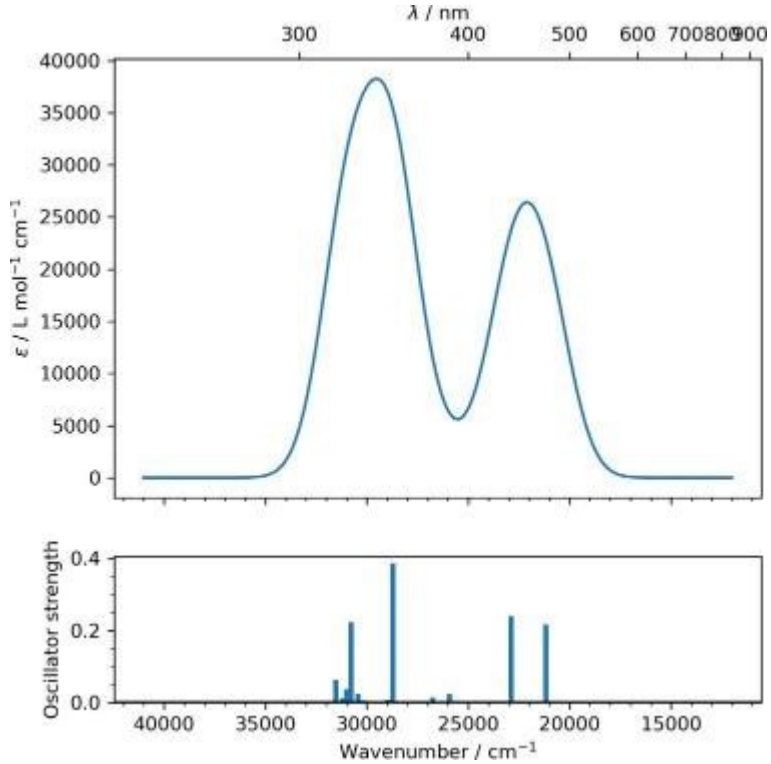

Figure S63. Calculated UV visible Absorption spectrum with a Gaussian broadening (FWHM = 3000 cm^{-1})

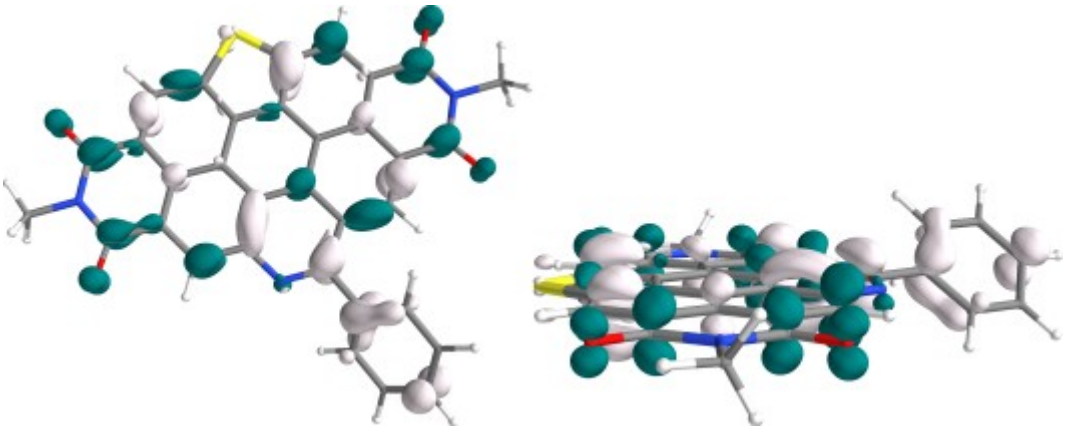

Figure S64.: Representation of the Electron Density Difference (S1-S0) from two points of view.

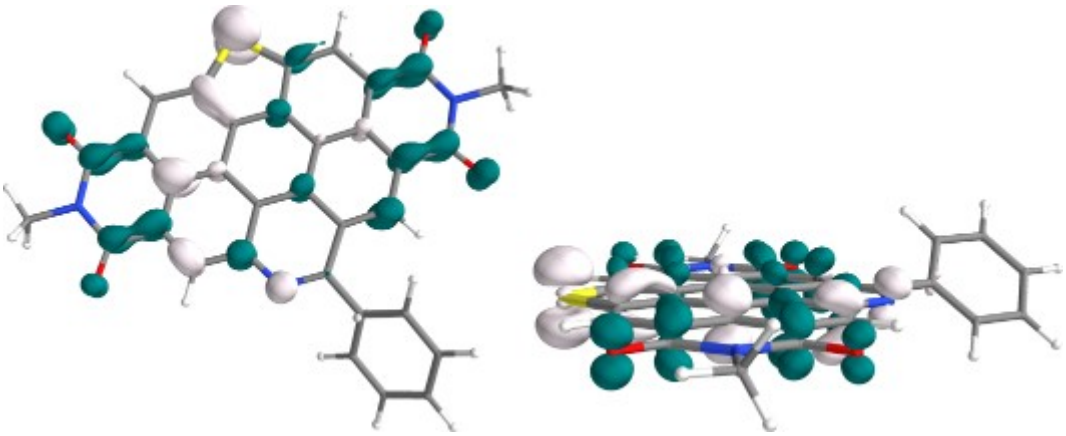

Figure S65. Representation of the Electron Density Difference (S2-S0) from two points of view.

E.S.	Symmetry	nm	cm^{-1}	*f*	R	Λ	d_{CT}	q_{CT}	Excitation description in %
1	Singlet-A	518	19299	0.234	23.8138	0.76	196.14	0.42	40->142 (5) 140->143 (2) 141->142 (90)

Table S11. Results concerning the calculated mono-electronic optimization excitation

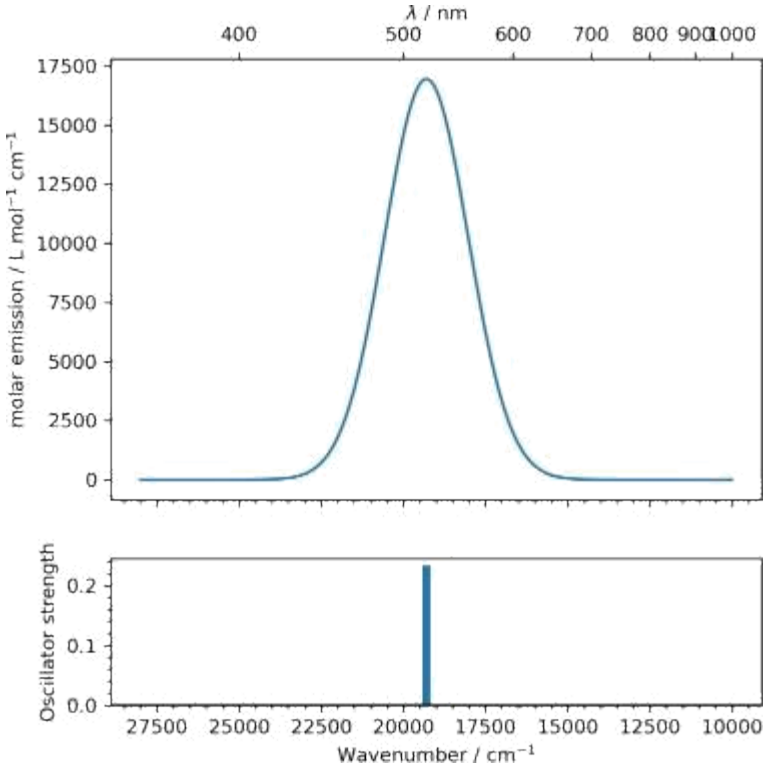

Figure S66. Calculated UV visible Emission spectrum with a Gaussian broadening (FWHM = 3000 cm-1)

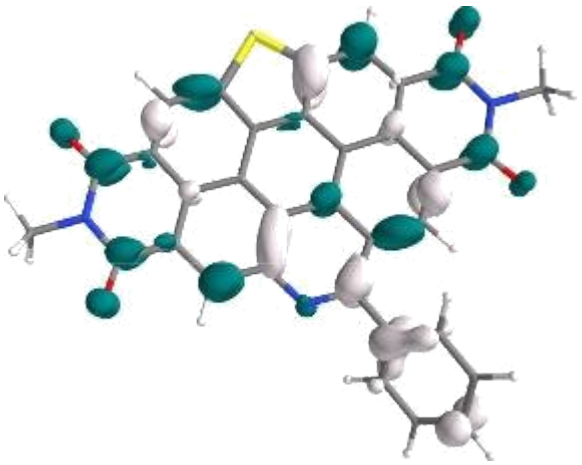

Figure S67. Representation of the Electron Density Difference (S1-GS) after optimization of the excited state. The excited electron and the hole regions are indicated by respectively white and blue surfaces to ease comparison with the corresponding absorption transition.

Atom	X	Y	Z
C	-3.1703	3.7908	0.8297
C	-1.9850	3.8059	0.0605
C	-1.6170	5.0092	-0.5907
C	-2.4260	6.1310	-0.5131
C	-3.6038	6.0952	0.2432

C	-3.9641	4.9247	0.9230
C	-1.0912	2.6409	-0.0433
C	-1.5825	1.2635	-0.0426
C	-0.5680	0.2655	0.0294
C	0.7963	0.6274	0.0373
C	1.1677	2.0040	-0.0599
N	0.2046	2.9588	-0.1089
C	-0.9208	-1.1057	0.0521
C	-2.2580	-1.5381	-0.0108
C	-3.2590	-0.5463	-0.1094
C	-2.9196	0.8212	-0.1406
C	-4.6636	-0.9755	-0.1942
N	-4.9014	-2.3578	-0.1629
C	-3.9270	-3.3778	-0.0745
C	-2.5243	-2.9379	-0.0013
C	0.0859	-2.0692	0.1047
C	-0.1565	-3.4580	0.1075
C	-1.4859	-3.8973	0.0605
C	1.8007	-0.3612	0.0733
C	1.4261	-1.7051	0.1168
C	3.1734	-0.0410	0.0333
C	3.5350	1.3394	-0.0505
C	2.5542	2.3288	-0.1008
C	4.1063	-1.0995	0.0595
C	3.6982	-2.4681	0.1070
C	2.3396	-2.7699	0.1303
C	5.5407	-0.7709	0.0222
N	5.8694	0.5982	-0.0456
C	4.9675	1.6772	-0.0922
O	-4.2506	-4.5582	-0.0626
O	-5.5989	-0.1878	-0.2811
C	-6.3108	-2.7605	-0.2365
O	6.4119	-1.6315	0.0477
C	7.2904	0.9625	-0.0832
O	5.3865	2.8247	-0.1632
H	4.4766	-3.2225	0.1129
S	1.4072	-4.3108	0.1438
H	2.8538	3.3682	-0.1683
H	-1.7614	-4.9454	0.0582

H	-3.7370	1.5173	-0.2763
H	-0.6978	5.0246	-1.1625
H	-2.1440	7.0380	-1.0371
H	-4.8623	4.9043	1.5306
H	-3.4404	2.9044	1.3894
H	7.8737	0.0472	-0.0248
H	7.5100	1.4995	-1.0089
H	7.5225	1.6233	0.7547
H	-6.3525	-3.8453	-0.1826
H	-6.8655	-2.3114	0.5902
H	-6.7490	-2.4056	-1.1722
H	-4.2334	6.9764	0.3113
C	-1.9628	-5.0659	0.0141
N	-1.1747	-5.7864	-0.2106
C	-2.2352	-5.1553	1.0729
C	-2.8368	-5.3058	-0.5976

Table S12. Converged cartesian atomic coordinates in Angstroms

Compound 4

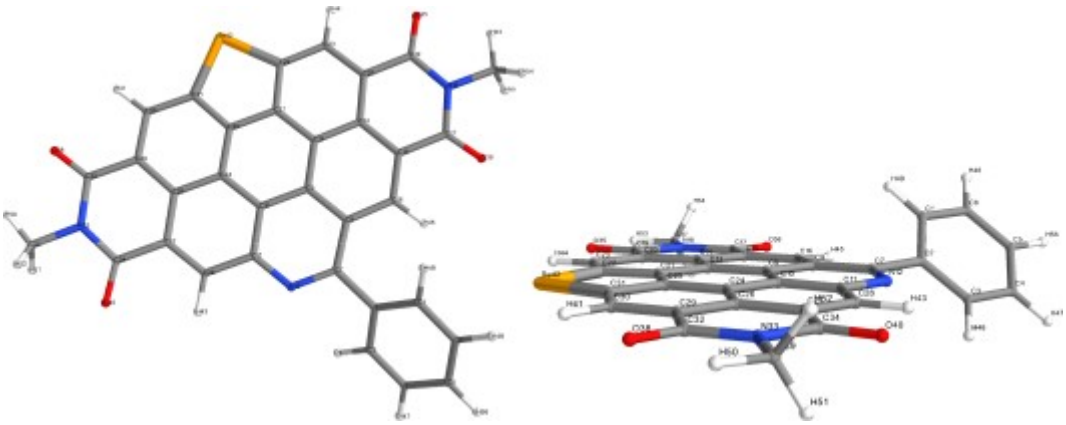

Figure S31. Chemical structure diagram with atomic numbering from two points of view.

Formula	C33H15N3O4Se	
Charge	0	
Spin multiplicity	1	
Total molecular energy		-4131.56181 hartrees
HOMO number		150
LUMO+1 energies		-2.55 eV
LUMO energies		-3.60 eV

HOMO energies	-6.52 eV
HOMO-1 energies	-6.74 eV
Geometry optimization specific results	
Converged nuclear repulsion energy	5004.50816 Hartrees
Frequency and Thermochemistry specific results	
Enthalpy at 298.15 K	-4131.12987 Hartrees
Gibbs free energy at 298.15 K	-4131.22073 Hartrees
Entropy at 298.15 K	0.00030 Hartrees

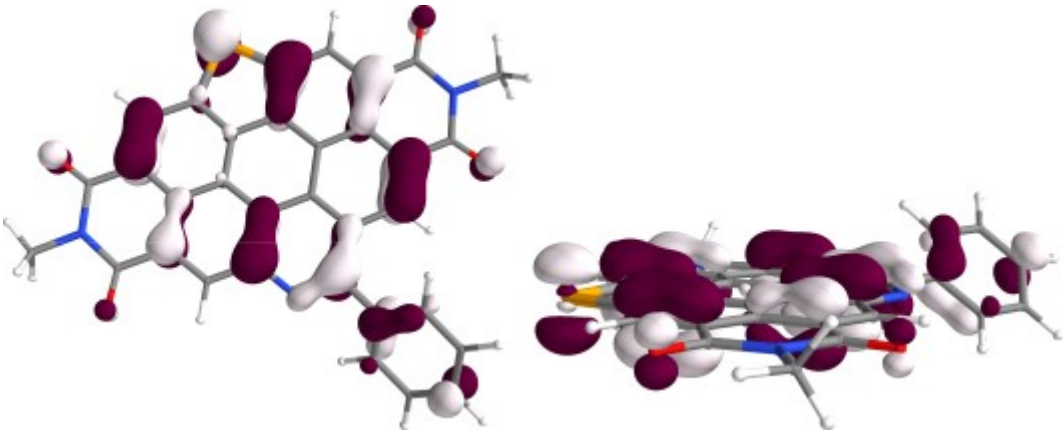

Figure S68. Representation of the HOMO from two points of view.

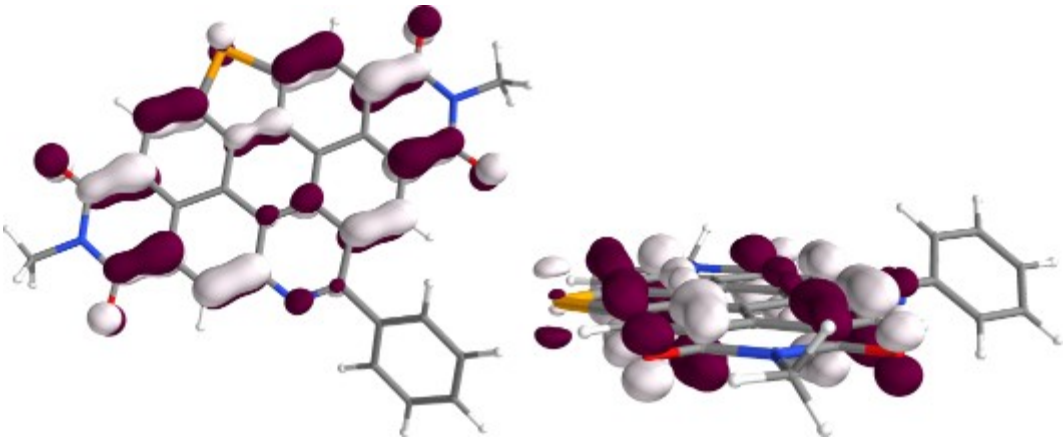

Figure S68. Representation of the LUMO from two points of view.

E.S.	Symmetry	nm	cm^{-1}	*f*	R	Λ	d_{CT}	q_{CT}	Excitation description : initial OM - ending OM (% if > 5%)-
1	Singlet-A	478	20890	0.193	10.0	0.76	124.73	0.41	149-151(11); 150-151(83);
2	Singlet-A	444	22510	0.268	1.8	0.74	140.57	0.44	149-151(80); 150-151(11);
3	Singlet-A	388	25736	0.031	-2.4	0.40	559.02	0.76	148-151(94);

4	Singlet-A	375	26657	0.006	-2.6	0.24	636.63	0.86	147-151(93);
5	Singlet-A	370	27014	0.000	-0.6	0.32	549.97	0.81	146-151(88);
6	Singlet-A	365	27368	0.000	1.4	0.33	539.77	0.79	145-151(89);
7	Singlet-A	351	28472	0.003	-2.2	0.48	253.34	0.66	143-151(32); 144-151(58);
8	Singlet-A	349	28631	0.384	16.7	0.65	248.20	0.45	150-152(76);
9	Singlet-A	344	28989	0.002	-2.7	0.53	209.37	0.65	141-151(11); 143-151(54); 144-151(28);
10	Singlet-A	333	29983	0.009	3.9	0.64	146.48	0.45	140-151(8); 150-153(61); 150-154(17);
11	Singlet-A	330	30215	0.196	24.5	0.59	387.73	0.41	149-152(54); 149-153(9); 150-154(13);

Table S13. Results concerning the calculated mono-electronic excitations.

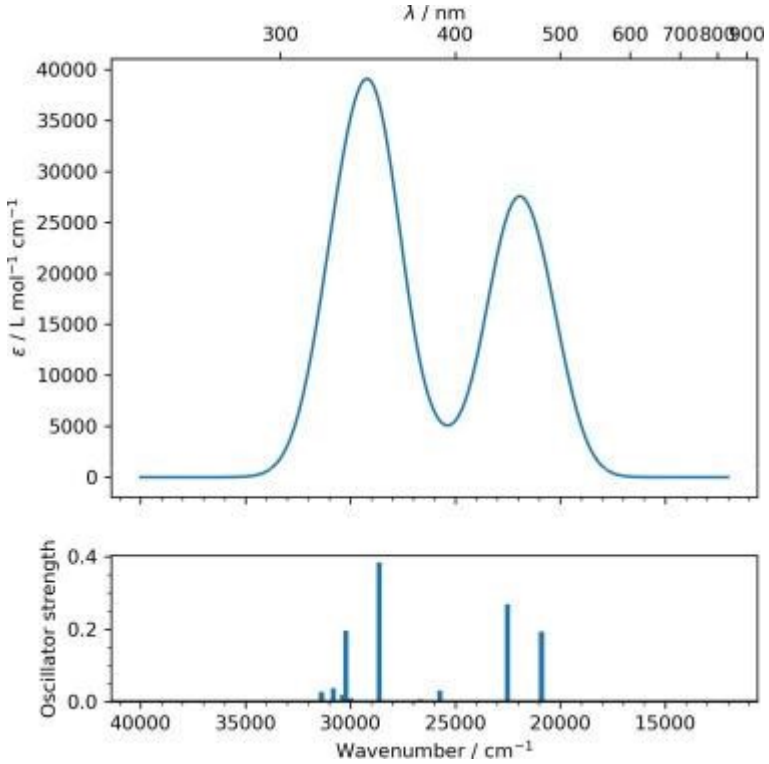

Figure S69. Calculated UV visible Absorption spectrum with a Gaussian broadening (FWHM = 3000 cm-1)

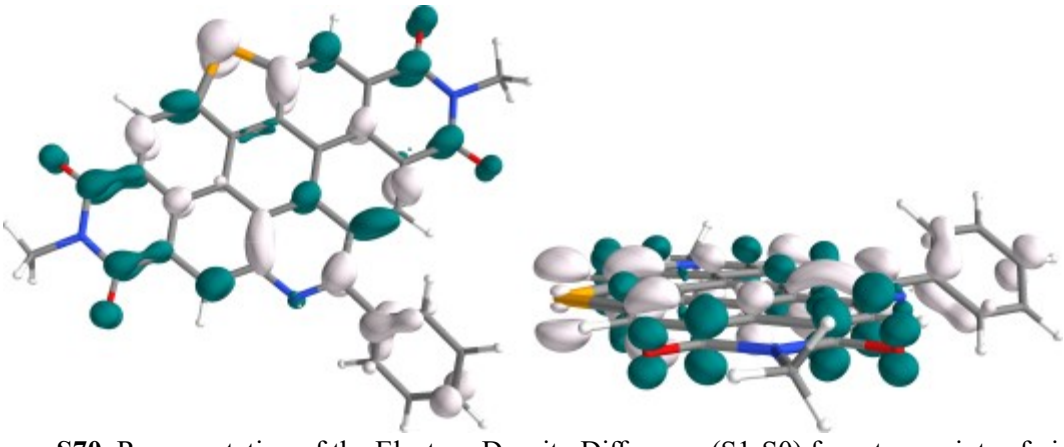

Figure S70. Representation of the Electron Density Difference (S1-S0) from two points of view.

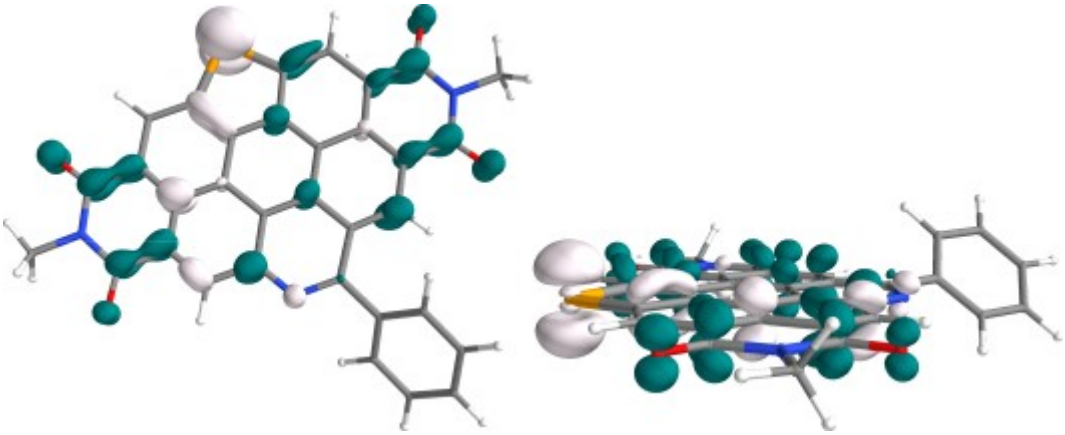

Figure S71. Representation of the Electron Density Difference (S2-S0) from two points of view.

E.S.	Symmetry	nm	cm^{-1}	*f*	R	Λ	d_{CT}	q_{CT}	Excitation description in %
2	Singlet-A	521	19170	0.229	22.733	0.76	49.78	0.43	149->151 (5) 149->152 (2) 150->151 (90)

Table S14. Results concerning the calculated mono-electronic optimization excitation

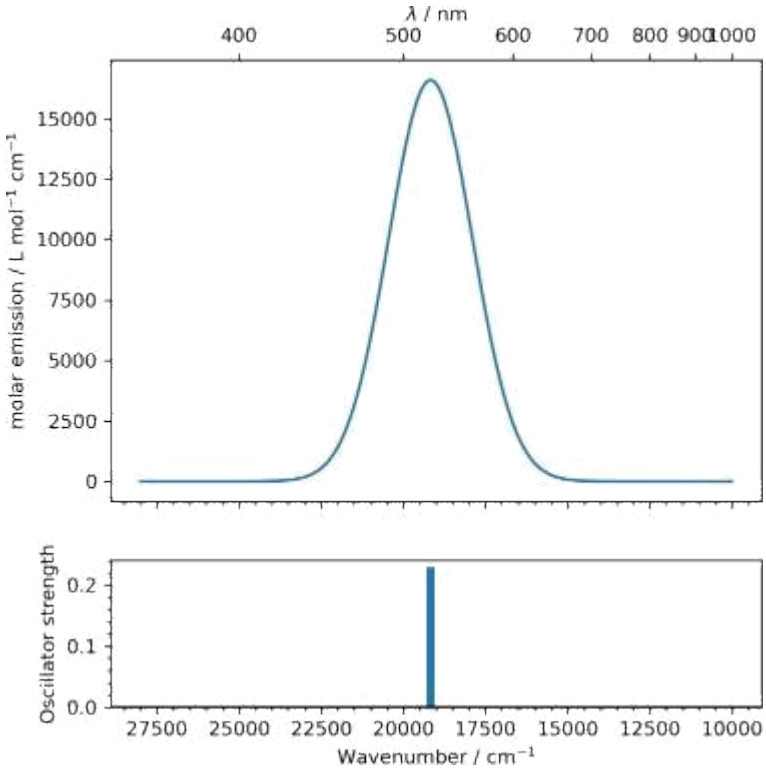

Figure S72. Calculated UV visible Emission spectrum with a Gaussian broadening (FWHM = 3000 cm-1)

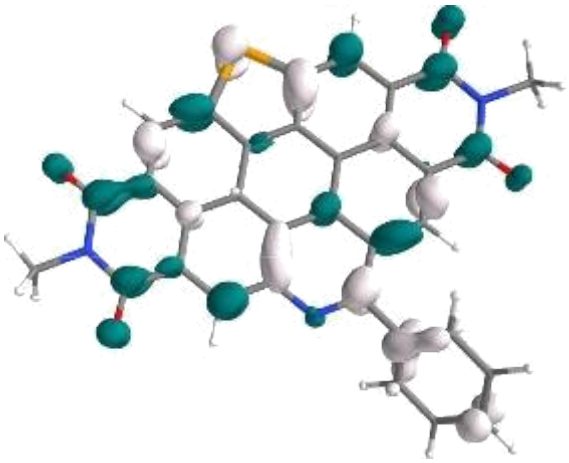

Figure S73. Representation of the Electron Density Difference (S1-GS) after optimization of the excited state. The excited electron and the hole regions are indicated by respectively white and blue surfaces to ease comparison with the corresponding absorption transition.

Atom	X	Y	Z
C	-3.5968	3.7281	0.8673
C	-2.4306	3.8563	0.0814
C	-2.1903	5.0867	-0.5749
C	-3.1041	6.1251	-0.4864
C	-4.2623	5.9774	0.2858
C	-4.4969	4.7797	0.9711
C	-1.4305	2.7810	-0.0349
C	-1.7893	1.3664	-0.0459
C	-0.6918	0.4583	0.0174
C	-0.1702	3.2150	-0.1030
N	-0.9208	-0.9404	0.0358
C	-2.2248	-1.4759	-0.0289
C	-3.3062	-0.5718	-0.1251
C	-3.0841	0.8167	-0.1489
C	-4.6727	-1.1106	-0.2156
C	-4.8029	-2.5061	-0.1909
N	-3.7503	-3.4421	-0.1000
C	-2.3893	-2.8890	-0.0226
C	0.1679	-1.8189	0.0865
C	0.0088	-3.2237	0.0905
C	-1.2805	-3.7587	0.0407
C	1.7240	0.0474	0.0576
C	1.4794	-1.3317	0.1001
C	3.0600	0.5090	0.0168

C	3.2879	1.9188	-0.0658
C	2.2193	2.8078	-0.1112
C	4.1002	-0.4406	0.0431
C	3.8314	-1.8387	0.0932
C	2.5162	-2.2812	0.1171
C	5.4947	0.0279	0.0048
C	5.6864	1.4208	-0.0664
N	4.6791	2.4003	-0.1099
C	-3.9752	-4.6457	-0.0901
O	-5.6661	-0.3976	-0.3023
O	-6.1751	-3.0195	-0.2726
C	6.4461	-0.7436	0.0319
O	7.0633	1.9263	-0.1068
C	4.9776	3.5850	-0.1803
O	4.6830	-2.5097	0.1018
H	1.7265	-4.0328	0.1375
Se	2.4148	3.8718	-0.1758
H	-1.4733	-4.8254	0.0385
H	-3.9554	1.4448	-0.2809
H	-1.2849	5.1916	-1.1593
H	-2.9184	7.0542	-1.0148
H	-5.3801	4.6722	1.5915
H	-3.7714	2.8207	1.4316
H	7.7353	1.0734	-0.0586
H	7.2222	2.4906	-1.0285
H	7.2329	2.5998	0.7362
H	-6.1291	-4.1047	-0.2313
H	-6.7657	-2.6266	0.5579
H	-6.6384	-2.6893	-1.2050
H	-4.9732	6.7937	0.3618
H	-6.7490	-2.4056	-1.1722
H	-4.2334	6.9764	0.3113
C	-1.9628	-5.0659	0.0141
N	-1.1747	-5.7864	-0.2106
C	-2.2352	-5.1553	1.0729
C	-2.8368	-5.3058	-0.5976

Table S15. Converged cartesian atomic coordinates in Angstroms

13. References

1. A. Goujon, L. Rocard, T. Cauchy and P. Hudhomme, *J. Org. Chem.*, 2020, **85**, 7218.
2. L. Rocard, D. Hatych, T. Chartier, T. Cauchy and P. Hudhomme, *Eur. J. Org. Chem.*, 2019, **47**, 7635.
3. H. Langhals and S. Kirner, *Eur. J. Org. Chem.*, 2000, **2000**, 365.
4. K. Wang, P. Xia, K. Wang, X. You, M. Wu, H. Huang, D. Wu and J. Xia, *ACS App. Mater. Interfaces*, 2020, **12**, 9528-9536.
5. U. Vongsaysy, B. Pavageau, G. Wantz, D. M. Bassani, L. Servant and H. Aziz, *Adv. Energy Mater.*, 2014, **4**, 1300752.